RM No. L7D08a

RESEARCH MEMORANDUM

AERODYNAMIC FORCE CHARACTERISTICS AT HIGH SPEEDS OF A FULL-SCALE HORIZONTAL TAIL SURFACE TESTED IN THE LANGLEY 16-FOOT HIGH-SPEED TUNNEL

By

Carl F. Schueller, Gerald Hieser, and Morton Cooper

Langley Memorial Aeronautical Laboratory
Langley Field, Va.

NATIONAL ADVISORY COMMITTEE FOR AERONAUTICS

WASHINGTON

June 9, 1947

NACA RM No. L7D08a

NATIONAL ADVISORY COMMITTEE FOR AERONAUTICS

RESEARCH MEMORANDUM

AERODYNAMIC FORCE CHARACTERISTICS AT HIGH SPEEDS OF A FULL-SCALE HORIZONTAL TAIL SURFACE TESTED IN THE LANGLEY 16-FOOT HIGH-SPEED TUNNEL

By Carl F. Schueller, Gerald Hieser, and Morton Cooper

SUMMARY

Tests have been conducted in the Langley 16-foot high-speed tunnel to determine the aerodynamic characteristics at high speeds of a full-scale horizontal tail surface. The tests were carried to a maximum Mach number of 0.68 except for model configurations at which the maximum allowable loads were reached at lower speeds.

The elevator hinge-moment parameter $C_{h_{\delta_e}}$ increased more rapidly and the parameter C_{h_α} less rapidly with increasing Mach number than would be predicted by the use of Glauert's factor, C_{h_α} increasing from -0.0012 to -0.0015 and $C_{h_{\delta_e}}$ increasing from -0.0051 to -0.0069 between $M = 0.20$ and $M = 0.68$. The elevator effectiveness $\partial\alpha/\partial\delta_e$ decreased from 0.538 to 0.415 between $M = 0.20$ and 0.68, because C_{L_α} increased much more rapidly than did $C_{L_{\delta_e}}$ with increasing Mach number. The elevator trim-tab-effectiveness parameter $\partial\delta_e/\partial\delta_t$ decreased from 0.434 to 0.335 between $M = 0.20$ and 0.60. However, this decrease occurred because $C_{h_{\delta_e}}$ increased more rapidly than did $C_{h_{\delta_t}}$ with increasing Mach number.

INTRODUCTION

A full-scale semispan left-hand horizontal tail surface of a high-speed airplane constructed according to present-day production methods was tested in the Langley 16-foot high-speed tunnel. The purpose of this investigation was to determine the aerodynamic characteristics of the horizontal tail at high

speeds. The tests to determine the external pressure distribution and balance-chamber pressures are in the process of analysis and will be presented in a later report.

SYMBOLS

C_D drag coefficient $\left(\frac{D}{q_o S}\right)$

C_h hinge-moment coefficient $\left(\frac{H}{q_o \bar{c}_e^2 b_e}\right)$

C_L lift coefficient $\left(\frac{L}{q_o S}\right)$

C_m pitching-moment coefficient $\left(\frac{M_{c'/4}}{q_o S_{c'}}\right)$

D drag of horizontal semispan tail surface

H hinge moment of elevator

L lift of horizontal semispan tail surface

$M_{c'/4}$ pitching moment about the quarter-chord point of the mean aerodynamic chord

P pressure coefficient $\left(\frac{p - p_o}{q_o}\right)$

p static pressure at any point, pounds per square foot

q dynamic pressure, pounds per square foot $\left(\frac{1}{2}\rho V^2\right)$

V velocity, feet per second

ρ density, slugs per cubic feet

b span of model (7.5 ft)

S total area of horizontal semispan tail surface, (24.13 sq ft)

$\bar{c}_e$ root mean square of the elevator chord aft of the hinge line (0.975 ft)

c' mean aerodynamic chord (3.34 ft)

M Mach number

R test Reynolds number

α free-air angle of attack of stabilizer, degrees

α_T angle of attack of stabilizer uncorrected for wind-tunnel-wall interference, degrees

δ_e angle of elevator chord with respect to the stabilizer chord (trailing edge down is positive), degrees

δ_t angle of trim-tab chord with respect to the elevator chord (trailing edge down is positive), degrees

$$\frac{\partial \alpha}{\partial \delta_e} = \frac{C_{L\delta_e}}{C_{L\alpha}}$$

$$C_{L\alpha} = \left(\frac{\partial C_L}{\partial \alpha}\right)_{\delta_e,\ \delta_t}$$

$$C_{L\delta_e} = \left(\frac{\partial C_L}{\partial \delta_e}\right)_{\alpha,\ \delta_t}$$

$$C_{h\alpha} = \left(\frac{\partial C_h}{\partial \alpha}\right)_{\delta_e,\ \delta_t}$$

$$C_{h\delta_e} = \left(\frac{\partial C_h}{\partial \delta_e}\right)_{\alpha,\ \delta_t}$$

$$\left(\frac{\partial \delta_e}{\partial \delta_t}\right)_{C_h} = \left(\frac{C_{h\delta_t}}{C_{h\delta_e}}\right)_{\alpha}$$

$$C_{h\delta_t} = \left(\frac{\partial C_h}{\partial \delta_t}\right)_{\alpha,\ \delta_e}$$

The subscripts outside the parentheses represent the factors held constant in the determination of the parameters.

Subscripts:

e elevator

i internal

t trim tab

o free stream

APPARATUS AND METHODS

Test model.- The model was a full-scale left-hand horizontal tail surface of a high-speed airplane. The airfoil was a symmetrical section 10 percent thick having maximum thickness at 40 percent of the chord. Since a semispan model was used, it was necessary to locate the center line of the horizontal tail surfaco in the plane of the tunnel wall to produce air-flow conditions approximately corresponding to those of flight. This result was accomplished by adding a 5-inch stub wing to the root section of the tail surface. The model was installed in the tunnel in an inverted position as shown in figure 1. Figure 2 and table I present the physical characteristics of the tail surface.

The stabilizer was of metal construction. Flush-head rivets were used in order to obtain a smooth, continuous surface; however, surface irregularities existed as may be seen in figure 1. The stabilizer included a balance chambor which is shown in detail in figure 3. A rubberized fabric seal was located between the nose of the elevator balance plate and the stabilizer balance chamber to prevent air leakage from the high-pressure to low-pressure sides of the tail surface. The seal also extended around the hinge pockets to prevent loss of balance pressure at these points.

The elovator was flush riveted, metal covered, and did not contain any air vents or drain holes. The elevator was an internally balanced sealed type and included a balance plate attached to the elevator nose. The elevator contour was a straight taper aft of the hinge line.

The elevator was equipped with a trim tab, the main dimensions of which are shown in figure 2. The production tail included a 24-volt direct-current motor rated at 1/30 horsepower at

7500 revolutions per minute which was used to actuate the trim tab.

Hinge-moment measurement.- The elevator torque tube was extended through the tunnel flat and through two self-alining bearings which were mounted on the tunnel balance frame. The elevator hinge moments were transferred through the elevator torque tube to a 10-inch crank and then through a jack screw to a scale platform. (See fig. 5 of reference 1.) The platform scale was attached rigidly to the tunnel balance frame; and since all other related parts were also attached to the tunnel balance frame, there was no possibility of the hinge-moment measurements interfering with the lift, drag, and pitching-moment measurements. All force and moment data were recorded simultaneously.

Elevator-angle measurement.- The root elevator angle was determined by means of an autosyn. The transmitter was rigidly attached to the stabilizer rear spar at approximately the 0-inch station (center line of airplane). A small pinion gear located on the transmitter shaft was driven by a large gear sector which was mounted rigidly to the elevator torque tube. Thus all elevator deflections were multiplied by a gear ratio of 12:1. A calibrated dial provided a continuous visual reading of the indicated root elevator angle. However, because of twist in the torque tube between the root of the elevator (5-inch station) and the gear sector (0-inch station), the indicated angle was not the true elevator root angle. A correction for this twist was determined statically and was applied to the indicated elevator angle as the tests were being run. The zero reading of the autosyn indicator was checked periodically with a templet. This system measured the elevator root angle within $\pm 0.1^{\circ}$.

Trim-tab angle measurement.- The trim-tab root angles were determined by means of a slide-wire resistance position indicator which was fastened rigidly to the elevator at approximately the 5-inch station. As the trim-tab angle changed, the position of the pickup arm varied, changing the resistance in the circuit; the corresponding changes in current were indicated on a microammeter. The trim-tab angle was calibrated against the microammeter reading and this calibration was checked periodically. The trim-tab root angles are accurate within $\pm 0.25^{\circ}$.

The variation in hinge-moment coefficient with time was determined by photographing the hinge-moment scale at 32 frames per second. The trim-tab angle at any given time was then determined from these data and the basic trim-tab aerodynamic data.

Angle-of-attack measurement.- The angle of attack was measured with an autosyn set up similar to the elevator root angle indicator. The angle-of-attack indicator reading was checked periodically during the tests by means of an inclinometer. The stabilizer root angles of attack are accurate within ±0.05°.

TESTS

The general aerodynamic data were obtained for a Mach number range from 0.20 to 0.68 for angles of attack α of -3°, $-1\frac{1}{2}$°, 0°, $1\frac{1}{2}$°, 3°, and 6° and for elevator deflections δ_e of -17°, -13°, -9°, -6°, -4°, -2°, 0°, 2°, 4°, 6°, and 9°. Any combination of these variables was limited by the maximum allowable load on either the stabilizer, elevator, or tail surface as a unit based on three-fourths of the design limit load. The trim-tab tests were run for angles of attack of $-1\frac{1}{2}$°, 0°, and $1\frac{1}{2}$°, elevator angles of -5°, 0°, and 5°, trim-tab angles δ_t of -16°, -8°, 0° and 8° and Mach numbers of 0.20, 0.40, and 0.60. Additional tests were made to determine the rate of change of trim-tab angle with time. These tests were conducted at a Mach number of 0.50, a tunnel angle of attack of -1°, and an elevator angle of -5° from the neutral to the maximum positive and negative tab angles, and at a Mach number of 0.60, a tunnel angle of attack of 0° and an elevator angle of -5° from the neutral to the maximum positive ang negative tab angles.

REDUCTION OF DATA

The data presented in this report have been corrected for tunnel-wall effects by the use of the reflection plane theory given in reference 2. The projected frontal area of the model was small in comparison to the tunnel cross sectional area so that tunnel constriction corrections were found to be negligible. Also, corrections to pitching moment due to model and balance-frame deflections were found to be negligible.

The horizontal tail surface was installed in the tunnel in an inverted position, but the signs of all coefficients and angles are presented so that the data may be applied directly to the airplane in the usual sense. The corrected data were cross-plotted and the faired values at selected angles of attack, elevator angles, and trim-tab angles were then plotted against

Mach number. The average test dynamic pressures and average test Reynolds numbers corresponding to the test Mach numbers are shown in figure 4. The Reynolds number is based on the mean aerodynamic chord of 3.34 feet. The results are generally plotted against Mach number rather than velocity or dynamic pressure because it is considered likely that Mach number is the dominating variable. The effects shown in these plots, however, are not entirely compressibility effects as they also include changes due to distortion of the model under load.

The rate of change of trim-tab angle with time was determined by reducing the photographed hinge-moment data to coefficient form and using them in conjunction with the basic hinge-moment coefficient versus trim-tab angle curves for a nominal elevator angle of -5°.

RESULTS AND DISCUSSION

Basic Data

Effect of angle of attack.- The variation of the lift coefficient, drag coefficient, and pitching-moment coefficient over a wide range of angle of attack is shown in figure 5 for elevator angles of 0°, and -10° a trim-tab angle of 0°, and a Mach number of 0.20. This figure shows that for an elevator angle of 0°, $C_{L_{max}} = 0.9$ and $C_{D_{min}} = 0.007$. This minimum drag coefficient is considered to be satisfactorily low for a model of this type of construction.

Effect of Mach number.- The variation of the drag coefficient, lift coefficient, pitching-moment coefficient, and hinge-moment coefficient with Mach number is presented in figure 6 for a test range of angle of attack $\alpha = -3°$ to 6° and elevator angle $\delta_e = -17°$ to 9°. The drag coefficient increased with Mach number at all elevator angles and angles of attack. However, the increase was not large enough to indicate that the critical speed had been attained. The lift and pitching-moment coefficients do not increase at all conditions as would be predicted by the use of Glauert's factor $(1 - M^2)^{-1/2}$. This result can be partially attributed to elevator twist, stabilizer twist, or both. The elevator hinge-moment coefficient increased with Mach number throughout the range of the tests. The increase is more rapid than would be predicted by Glauert's factor, probably because of structural deflections.

Figure 6(c) shows that for an angle of attack $\alpha = 0°$, elevator angle $\delta_e = 0°$, trim-tab angle $\delta_t = 0°$, and Mach

number $M = 0.2$, the lift coefficient equals 0.02 and the hinge-moment coefficient equals -0.009. Since the airfoil section is symmetrical, these values might indicate discrepancies in the test data. However, close examination of the model indicated the following construction errors which probably account for the discrepancy: The elevator trailing-edge angle varied from 13.6° to 14.0° from root to tip, the elevator had a spanwise twist of approximately 0.8°, and the elevator lower surface had a cusp which at the 20-inch station was $\frac{1}{8}$-inch deep and $\frac{1}{16}$-inch deep at the 40-inch station. The center of the cusp was located at approximately $0.85\bar{c}_e$ and the length of the cusp was $0.30\bar{c}_e$.

Aerodynamic Parameters

Effect of Mach number.- The variation of C_{L_α} and $C_{L_{\delta_e}}$ with Mach number is presented in figure 7 and indicates that both parameters increase with increasing Mach number. The increase of C_{L_α} with Mach number is somewhat greater than would be predicted by Glauert's factor, and no critical condition exists up to Mach number $M = 0.68$. Application of the Young-Owen method for first-order compressibility effects on control hinge-moment coefficients, which consists of refinements to Glauert's factor for models of finite aspect ratio, yields results which differ only slightly from Glauert's factor for this model. Figure 7 shows that the elevator effectiveness which is defined as $\frac{C_{L_{\delta_e}}}{C_{L_\alpha}} = \frac{\partial\alpha}{\partial\delta_e}$ decreased from 0.538 at a Mach number of 0.20 to 0.415; at a Mach number of 0.68, however, it should be pointed out that this decrease in effectiveness is caused by the rapid increase in C_{L_α} and not a decrease in $C_{L_{\delta_e}}$ with increasing Mach number.

Figure 8 presents the variation of C_{h_α} and $C_{h_{\delta_e}}$ with Mach number. The hinge-moment parameter $C_{h_{\delta_e}}$ increased more rapidly with increasing Mach number than would be predicted by the use of Glauert's factor, while the parameter C_{h_α} increased less rapidly than would be predicted by Glauert's factor. This disagreement can be attributed in part to structural deflections and the limitations of the thin airfoil theory upon which Glauert's factor is based.

Figure 9 presents the variation of C_{m_α} and $C_{m_{\delta_e}}$ with Mach number. The pitching-moment parameter $C_{m_{\delta_e}}$ increased

more rapidly with Mach number than would be predicted by Glauert's factor while the parameter C_{m_α} increased as would be predicted by the use of Glauert's factor.

Elevator Trim-Tab Characteristics

Effect of Mach number.- Figure 10 shows the effect of Mach number on the aerodynamic characteristics of the tail surface for elevator trim-tab angles of 8° to -16°. The results are given for angles of attack of $-1\frac{1}{2}^\circ$, 0°, and $1\frac{1}{2}^\circ$ and elevator angles of -5°, 0°, and 5°. The dashed portion of the curves represent extrapolated data.

Elevator trim-tab effectiveness may be defined either as $C_{h_{\delta_t}}$ or $\frac{C_{h_{\delta_t}}}{C_{h_{\delta_e}}} = \frac{\partial \delta_e}{\partial \delta_t}$. The variation of these parameters with Mach number is shown in figure 11. The parameter $C_{h_{\delta_t}}$ shows a slight increase between a Mach number of 0.20 and 0.60, while $\partial\delta_e/\partial\delta_t$ shows a decrease from 0.434 at a Mach number of 0.20 to 0.355 at a Mach number of 0.60. However, it must be emphasized that this decrease results because $C_{h_{\delta_e}}$ increases more rapidly with Mach number than does $C_{h_{\delta_t}}$.

Rate of change of trim-tab angle with time.- The maximum elevator trim-tab angle that could be obtained with this tail surface under aerodynamic load and the rate of change of trim-tab angle with time under aerodynamic load were determined.

Figure 12(a) presents the variation of trim-tab angle with time from the neutral position to the maximum position at a Mach number of 0.60, tunnel angle of attack of 0°, and elevator angle of -5°. Over the linear portion of the curve, the rate of change of trim-tab angle with time is approximately 2.6° per second.

Figure 12(b) presents similar data for a Mach number of 0.50 at a tunnel angle of attack of 1° and an elevator angle of -5°. The rate of change of trim-tab angle with time is approximately 2.5° per second for this configuration.

Figures 13 and 14 present the variation of trim-tab angle with time from the neutral to maximum negative position for test conditions of Mach number of 0.60 tunnel angle of attack of 0°, and

an elevator angle of -5°; and a Mach number of 0.50, tunnel angle of attack of -1°, and an elevator angle of -5°, respectively. The rates of change of trim-tab angle with time are 2.2° and 2.6° per second, respectively.

Although a constant indicated elevator angle of -5° was maintained during the trim-tab angle versus time tests, the true elevator angle varied due to twist in the elevator hinge-moment measurement system under varying load. Therefore, the actual elevator angles which occurred during these runs are included in figures 12 to 14.

Effect of Mach Number and Angle of Attack on Lower Surface Skin Deflection

In order to determine the extent and approximate magnitude of skin deflection on the tail surface, a photographic study of the tail surface under various representative aerodynamic loads was made.

Figure 15 shows a view of the lower surface of the horizontal tail for no aerodynamic load. A comparison of figures 15 and 16 shows the effect of aerodynamic load on the lower-surface skin deflections for $\alpha_T = 0^\circ$, $\delta_e = -5^\circ$, $\delta_t = 0^\circ$, and $M = 0.60$. The skin bulges for this configuration are quite pronounced and occur across the entire stabilizer. The difference between the internal pressure in the stabilizer and free-stream static pressure is very low, amounting to approximately 0.035 pound per square inch. The deflection of the skin must therefore be attributed to weaknesses of the skin structure.

Figure 17 presents the skin deflections for tunnel angles of attack of 0° and -6° at $M = 0.40$, $\delta_e = 0^\circ$, and $\delta_t = 0^\circ$. For the zero angle-of-attack condition (fig. 17(a)) the loads on the tail are extremely small and, as a result, the skin bulges are of a very minor degree. For the tunnel angle of attack of -6° (fig. 17(b)) where the tail loading is high, the skin bulging is considerable and covers the entire tail surface. The difference between the internal pressure of the stabilizer and free-stream static pressure is only 0.016 pound per square inch.

The excessive amount of skin deflections of the horizontal tail under load may contribute to the increase in drag coefficient with Mach number which is shown in figure 6.

CONCLUSIONS

The following conclusions may be drawn from the investigation described in this report:

1. The hinge-moment parameter $C_{h_{\delta_e}}$ increased more rapidly and the parameter C_{h_α} less rapidly with increasing Mach number than would be predicted by the use of Glauert's factor, C_{h_α} increasing from -0.0012 to -0.0015 and $C_{h_{\delta_e}}$ increasing from -0.0051 to -0.0069 between $M = 0.20$ and 0.68.

2. Both C_{L_α} and $C_{L_{\delta_e}}$ increase with increasing Mach number. However, the elevator effectiveness parameter $\partial\alpha/\partial\delta_e$ decreased from 0.538 at $M = 0.20$ to 0.415 at $M = 0.68$ because C_{L_α} increases much more rapidly than $C_{L_{\delta_e}}$ with increasing Mach number.

3. The elevator trim-tab effectiveness parameter $C_{h_{\delta_t}}$ increases slightly with increasing Mach number. However, the elevator trim-tab effectiveness parameter $\partial\delta_e/\partial\delta_t$ shows a decrease from 0.434 at $M = 0.20$ to 0.355 at $M = 0.60$ because $C_{h_{\delta_e}}$ increases much more rapidly with increasing Mach number than does $C_{h_{\delta_t}}$.

Langley Memorial Aeronautical Laboratory
National Advisory Committee for Aeronautics
Langley Field, Va.

REFERENCES

1. Schueller, Carl F., and Korycinski, Peter F.: Effect of Fabric Deflection at High Speeds on the Aerodynamic Characteristics of the Horizontal Tail Surface of an SB2D-1 Airplane. NACA ARR No. L5F01a, 1945.

2. Swanson, Robert S., and Toll, Thomas A.: Jet-Boundary Corrections for Reflection-Plane Models in Rectangular Wind Tunnels. NACA ARR No. 3E22, 1943.

TABLE I

PHYSICAL CHARACTERISTICS OF THE HORIZONTAL TAIL SURFACE

[Symmetrical airfoil section, 10 percent thick]

Area of stabilizer, S_s, square feet	15.17
Area of elevator, S_f, square feet	8.56
Area of stub wing, S_p, square feet	1.715
Area of overhang, S_b, square feet	2.06
Area of elevator aft of hinge line, S_e, square feet	6.5
Area of tab, S_t, square feet	0.6
Span of elevator, b_f, feet	6.67
Aspect ratio, (b_w^2/s_w)	4.65
Taper ratio, (c_{tip}/c_{root})	0.560
Elevator hinge-line location, percent of total chord	70.3
Tab hinge-line location, percent of total chord	88.2 at station 13
Elevator overhang, S_b/S_e, percent	31.7
Mean tab chord, $\bar{c}_t$, feet	0.463

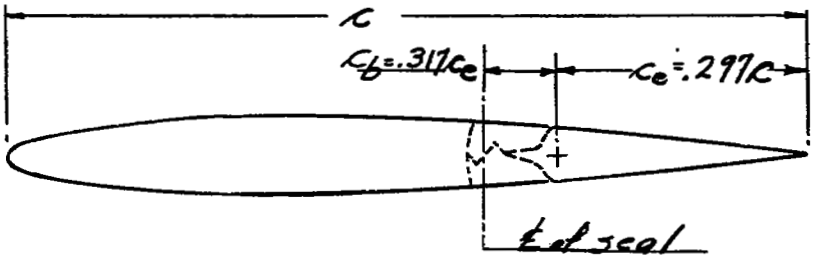

NATIONAL ADVISORY
COMMITTEE FOR AERONAUTICS.

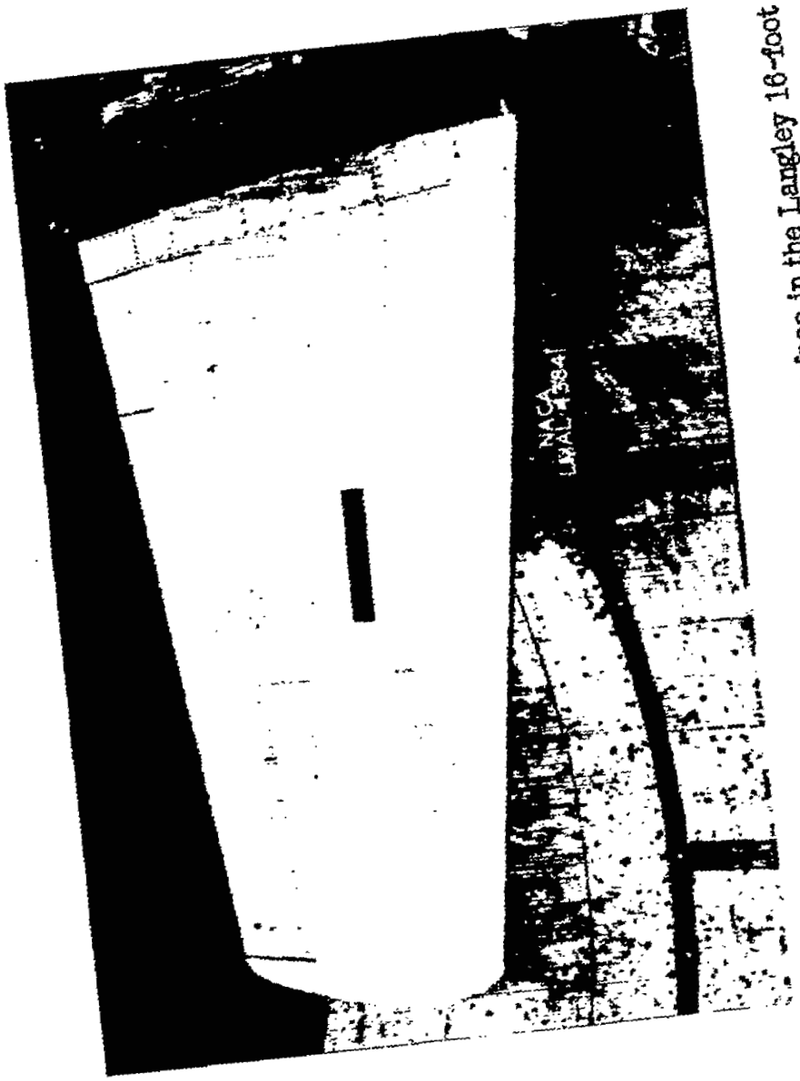

Figure 1.- General view of the horizontal tail surface in the Langley 16-foot high-speed tunnel.

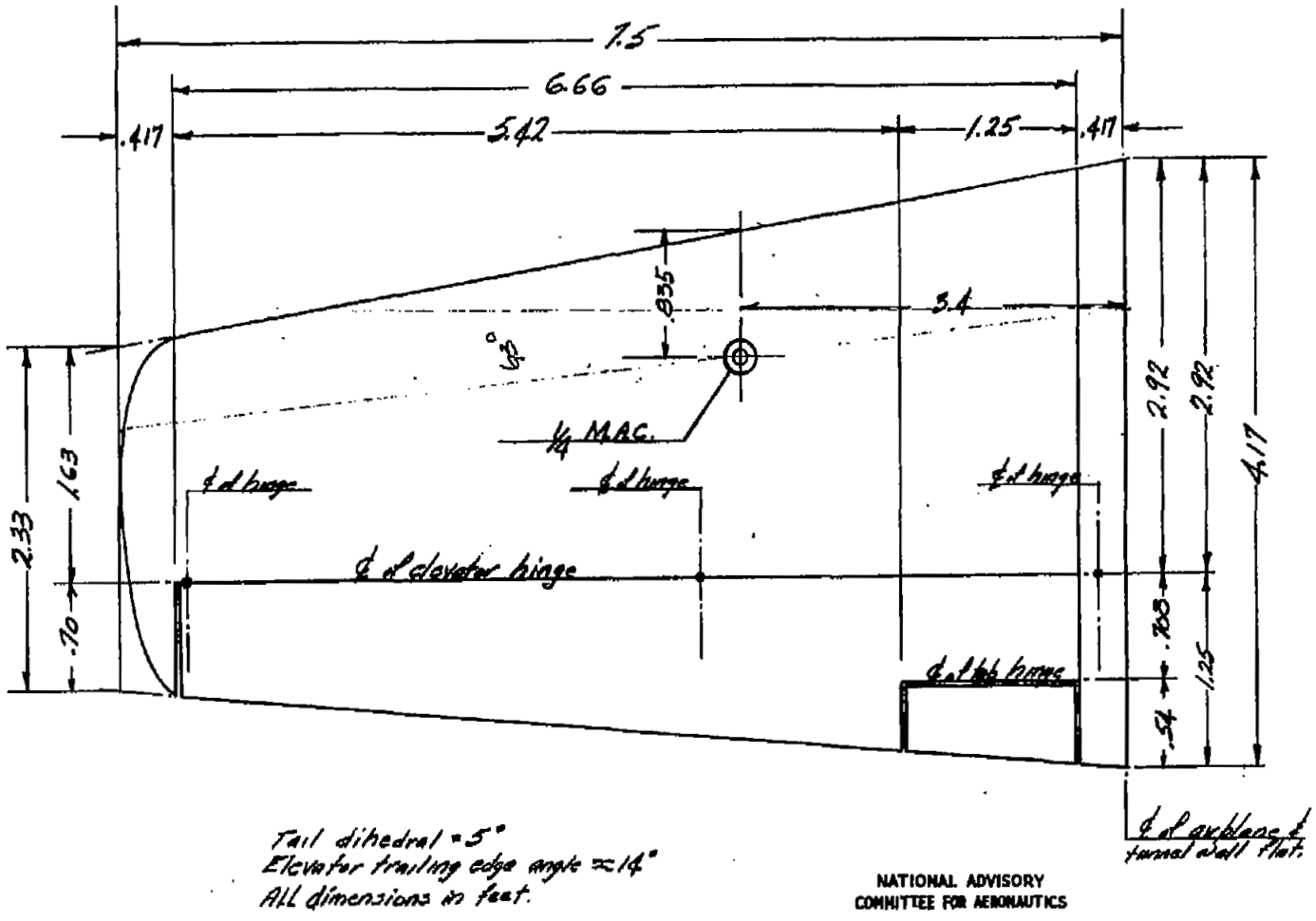

Figure 2.- General arrangement of the horizontal tail surface.

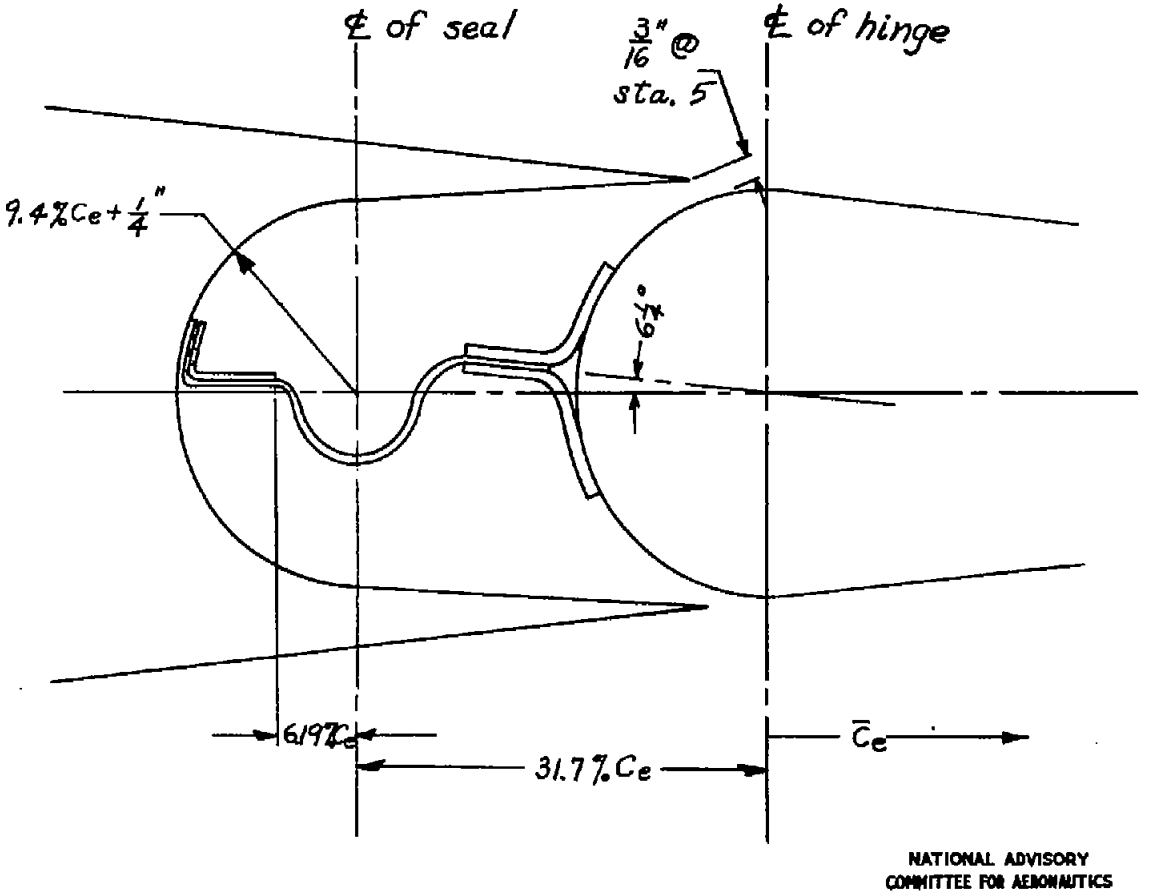

Figure 3.- Detail of balance chamber.

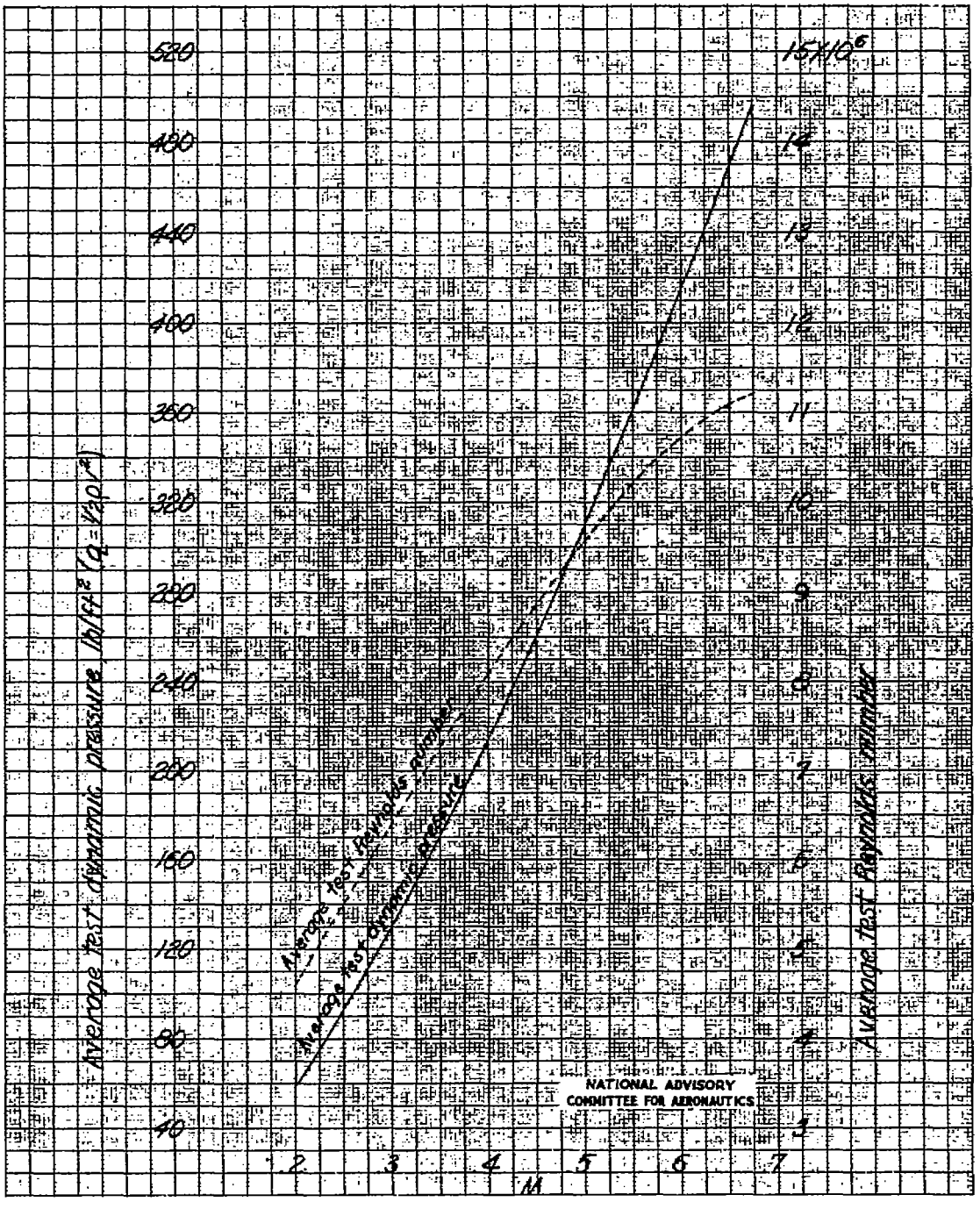

Figure 4.- Variation of the average test Reynolds number and dynamic pressure with test Mach number.

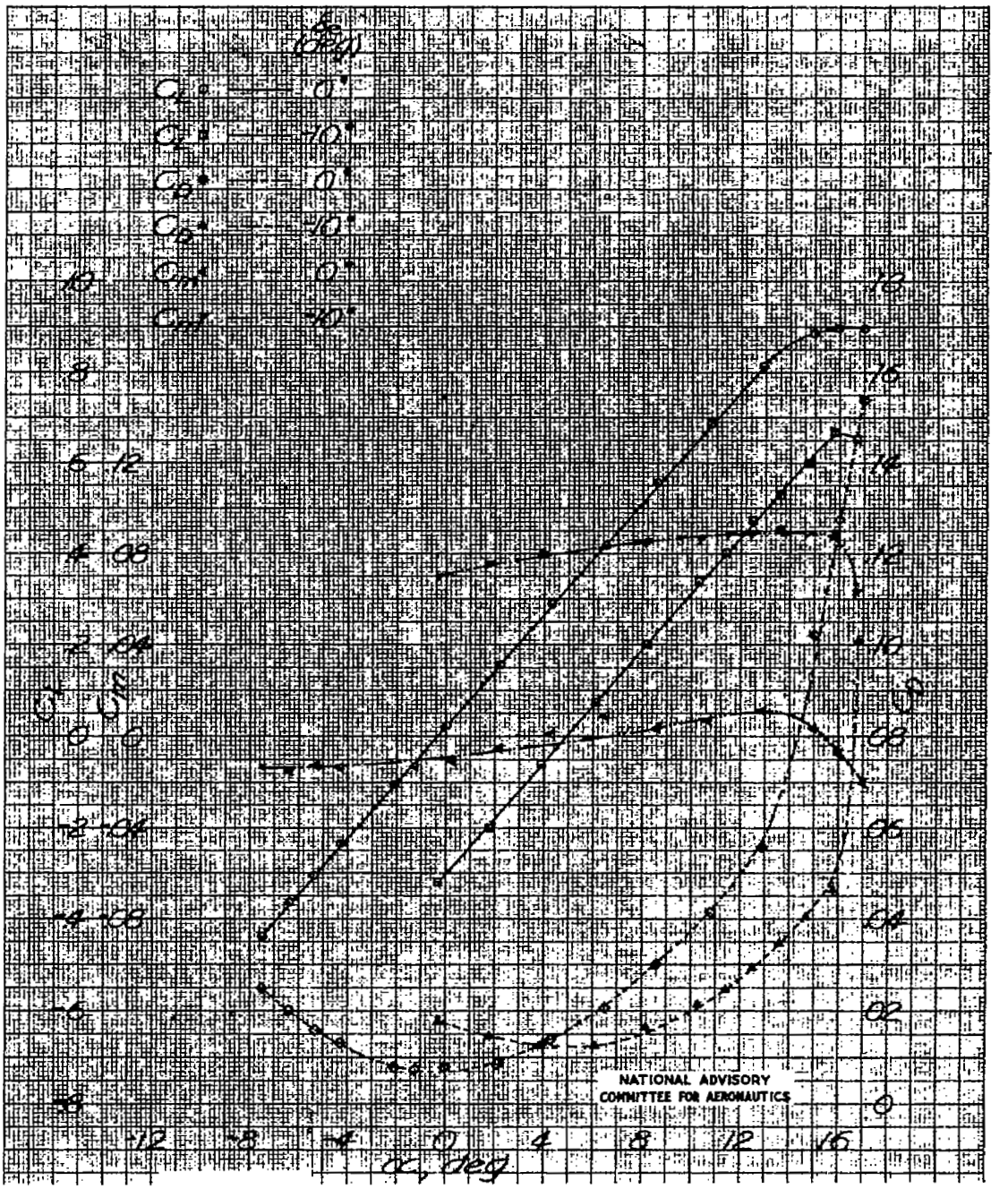

Figure 5.- Variation of the aerodynamic characteristics with angle of attack, M = 0.2, $\delta_t = 0^\circ$.

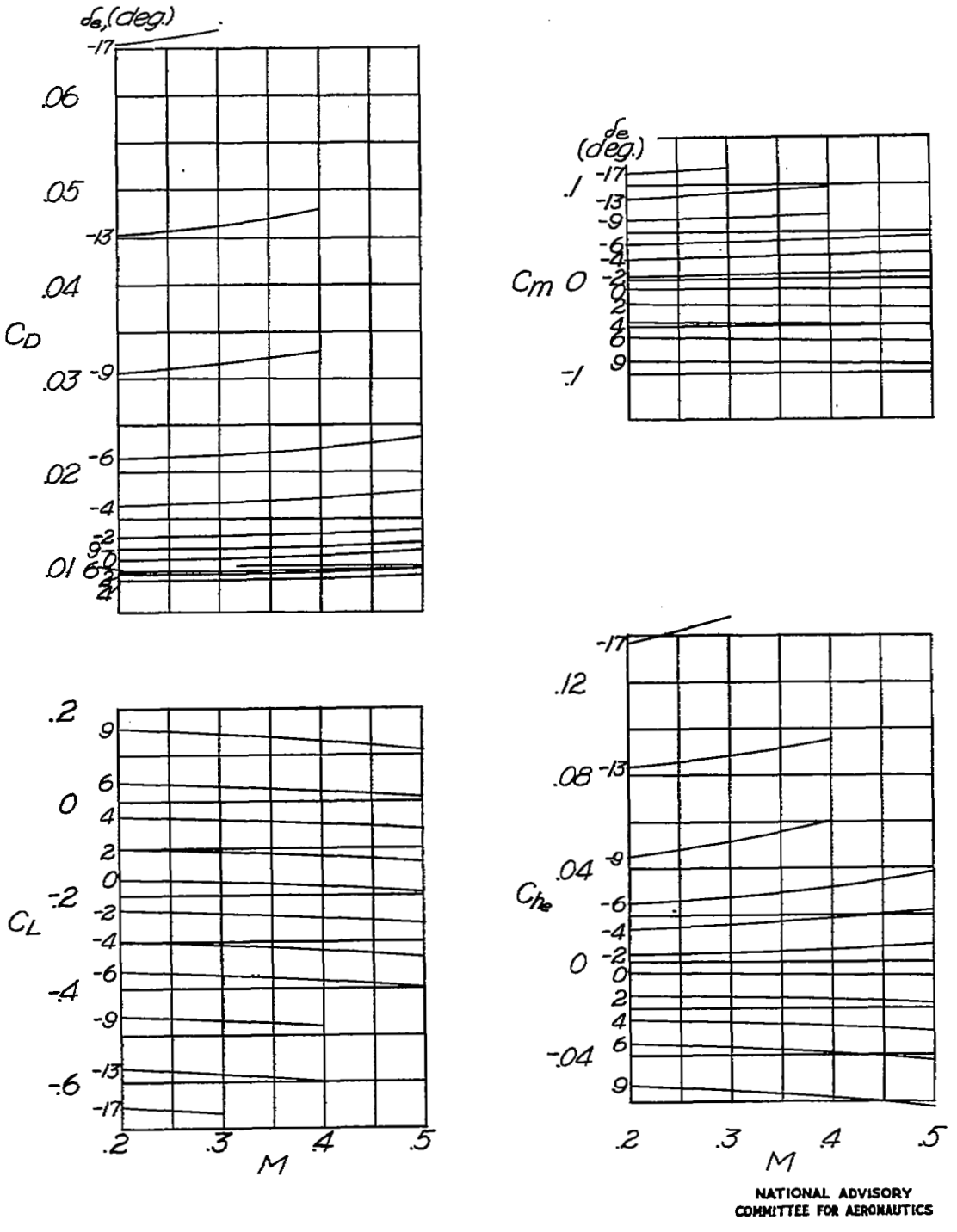

(a) Angle of attack, $\alpha = -3^{\circ}$.

Figure 6.- Variation of the aerodynamic characteristics with Mach number for a range of elevator angles and angles of attack.

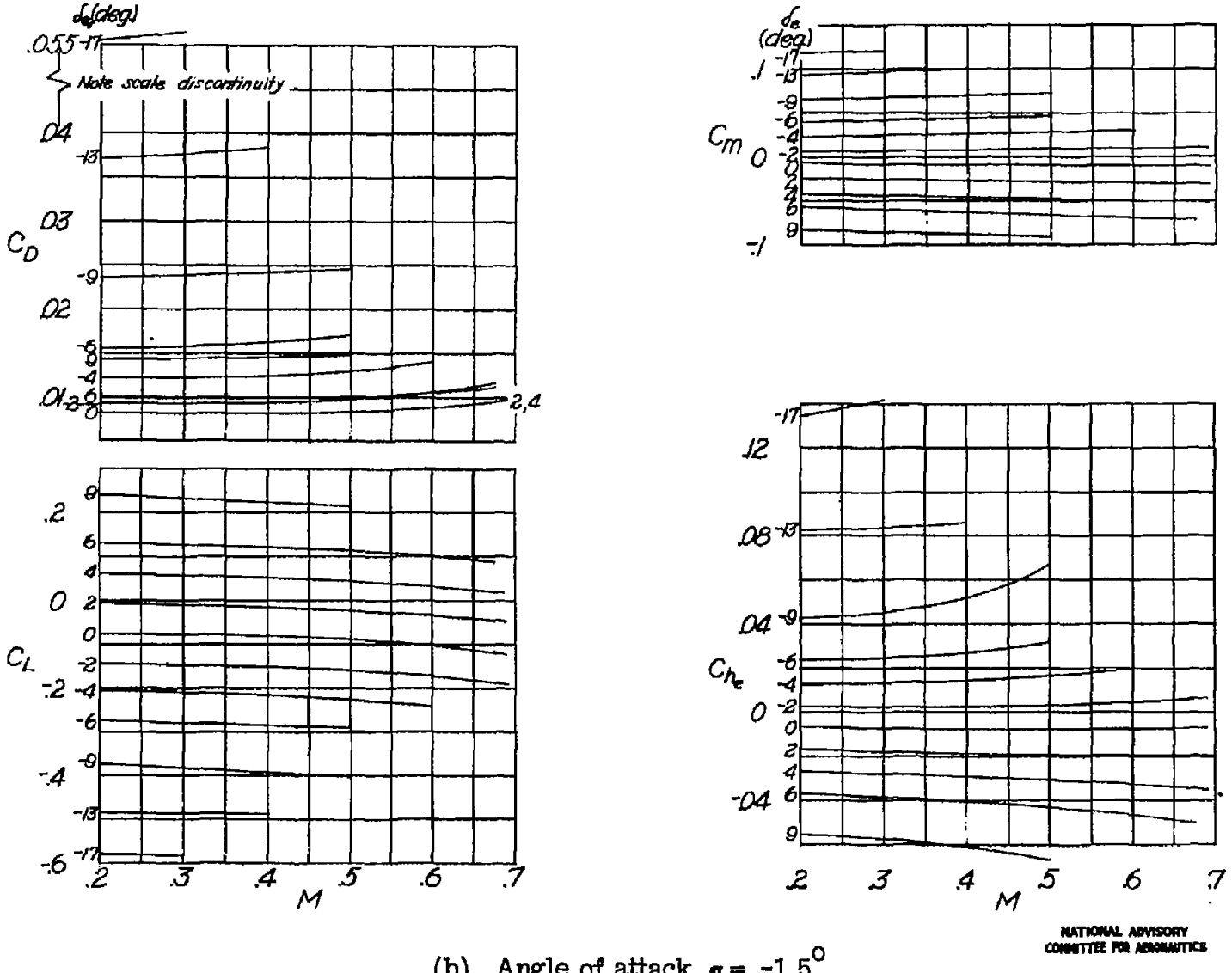

(b) Angle of attack, $\alpha = -1.5^{\circ}$.

Figure 6.- Continued.

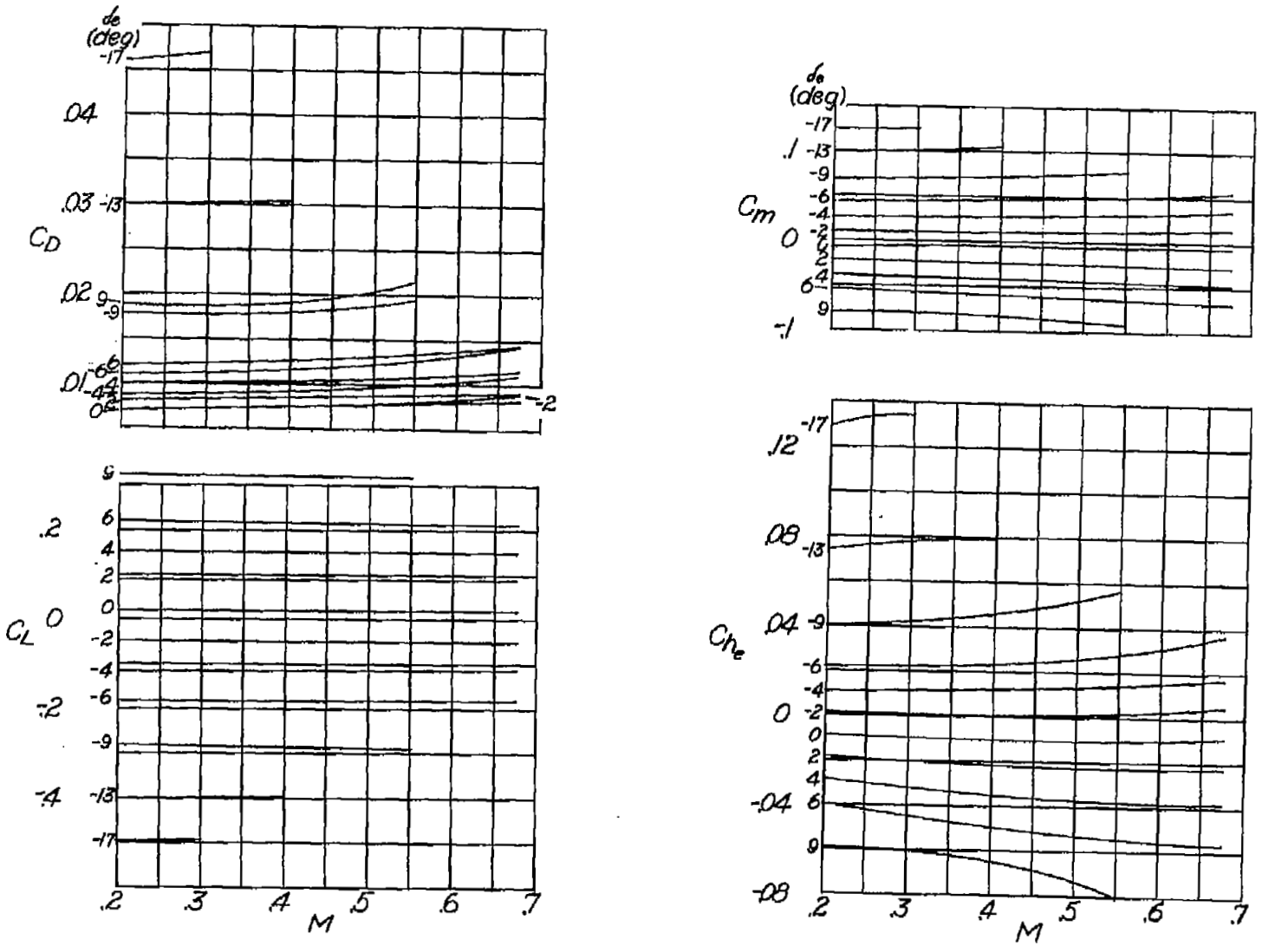

(c) Angle of attack, $\alpha = 0^\circ$.

Figure 6.- Continued.

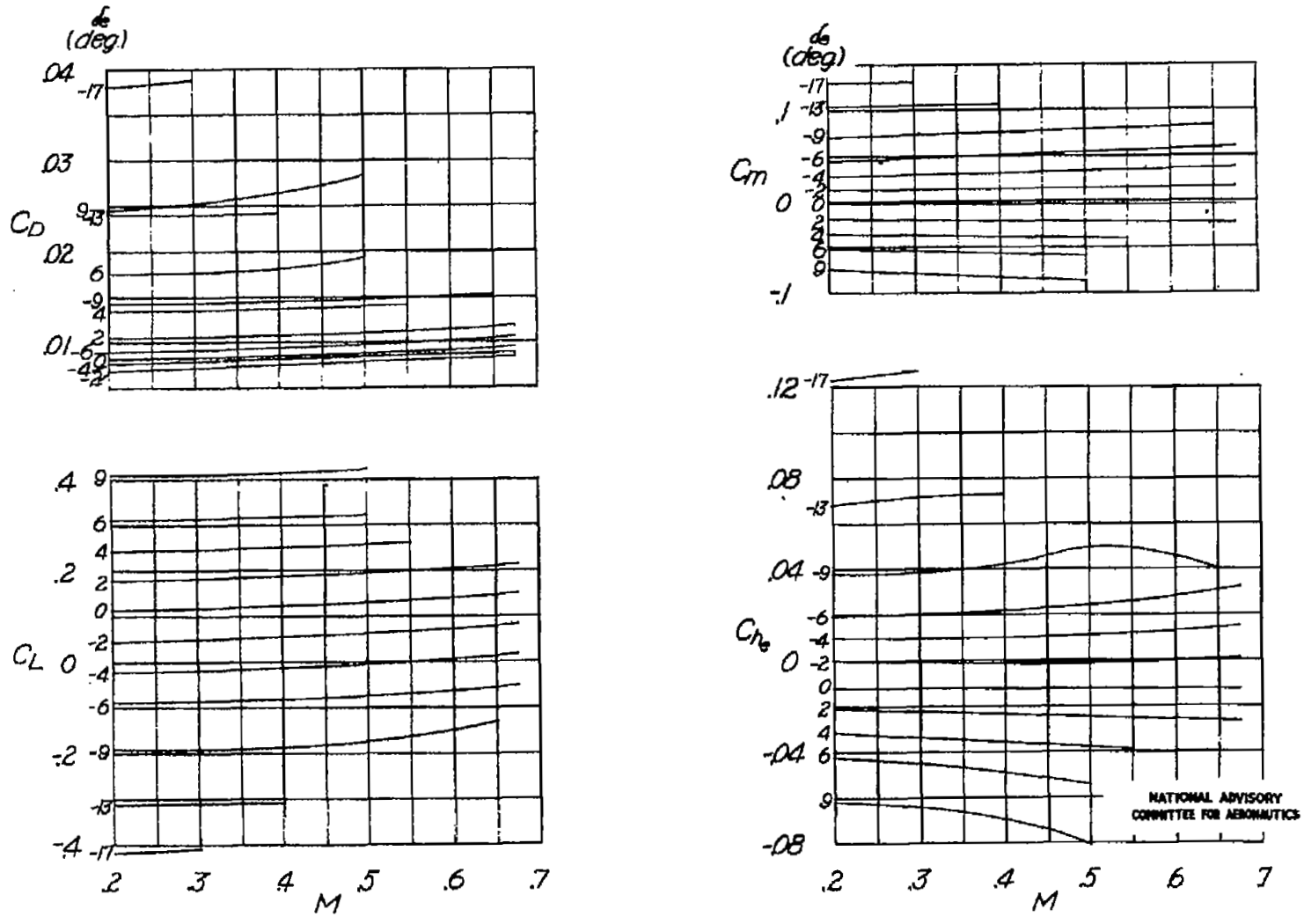

(d) Angle of attack, $\alpha = 1.5^{\circ}$

Figure 6.- Continued.

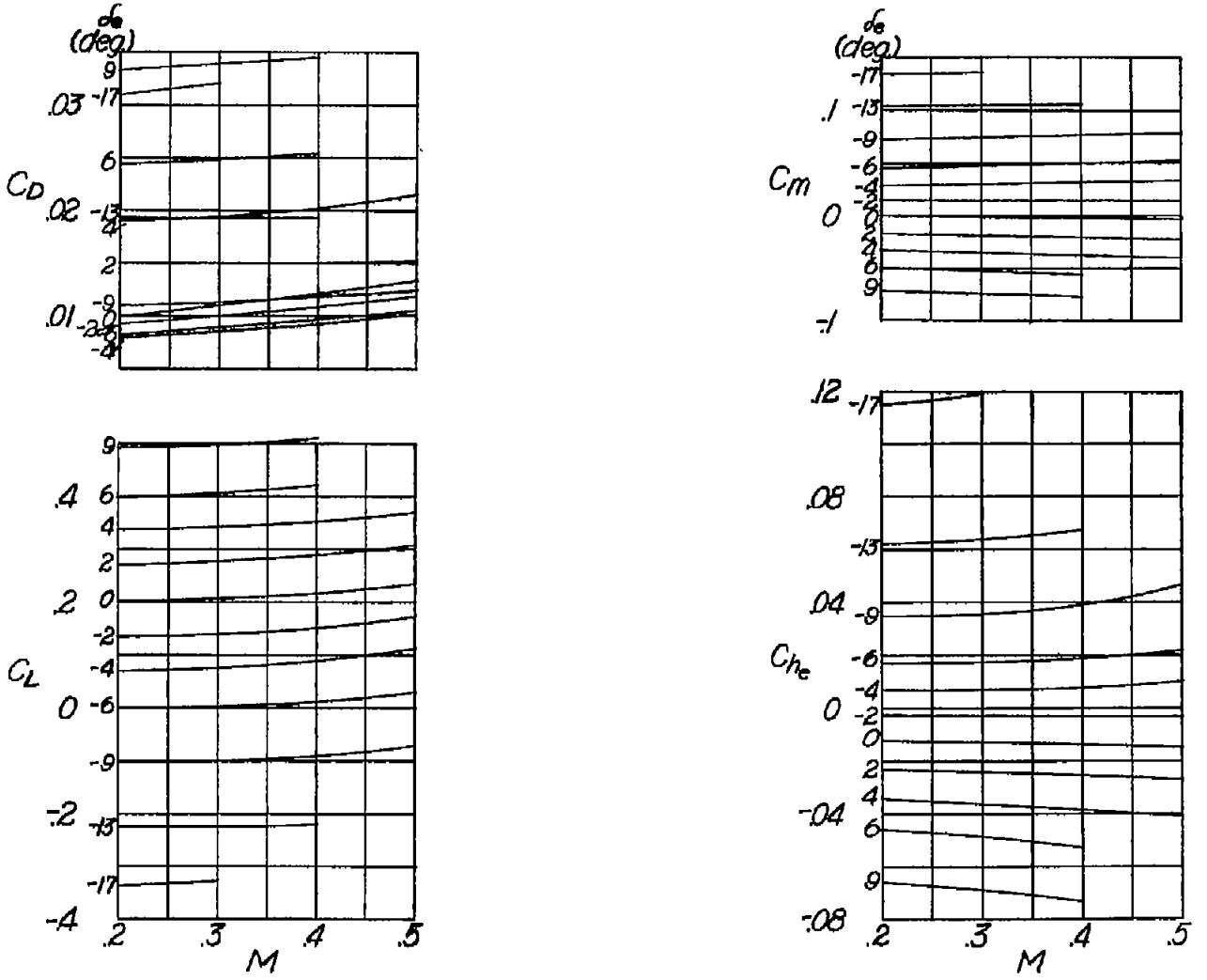

(e) Angle of attack, $\alpha = 3^\circ$.

Figure 6.- Continued.

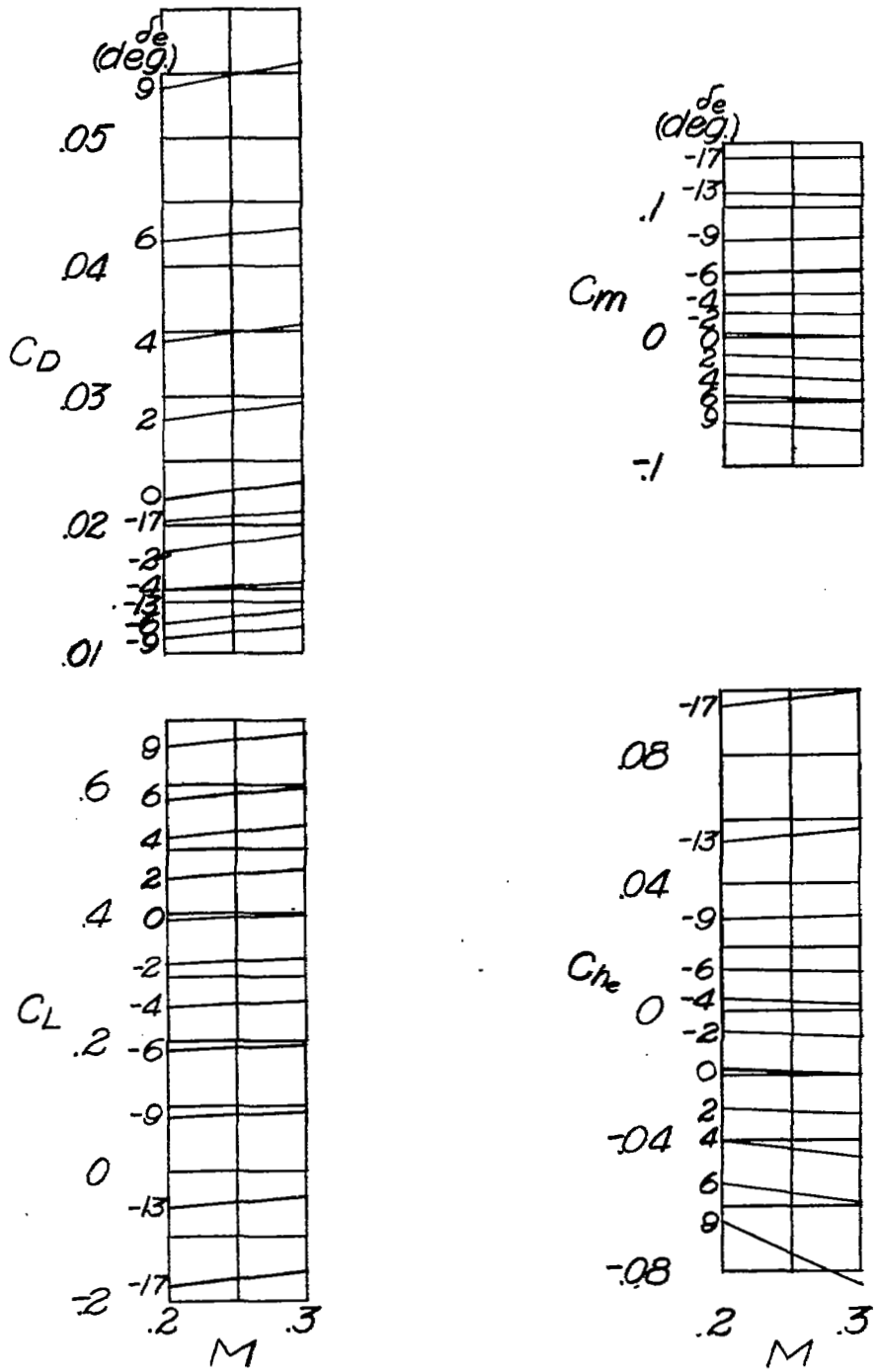

(f) Angle of attack, $\alpha = 6^\circ$.

NATIONAL ADVISORY COMMITTEE FOR AERONAUTICS

Figure 6.- Concluded.

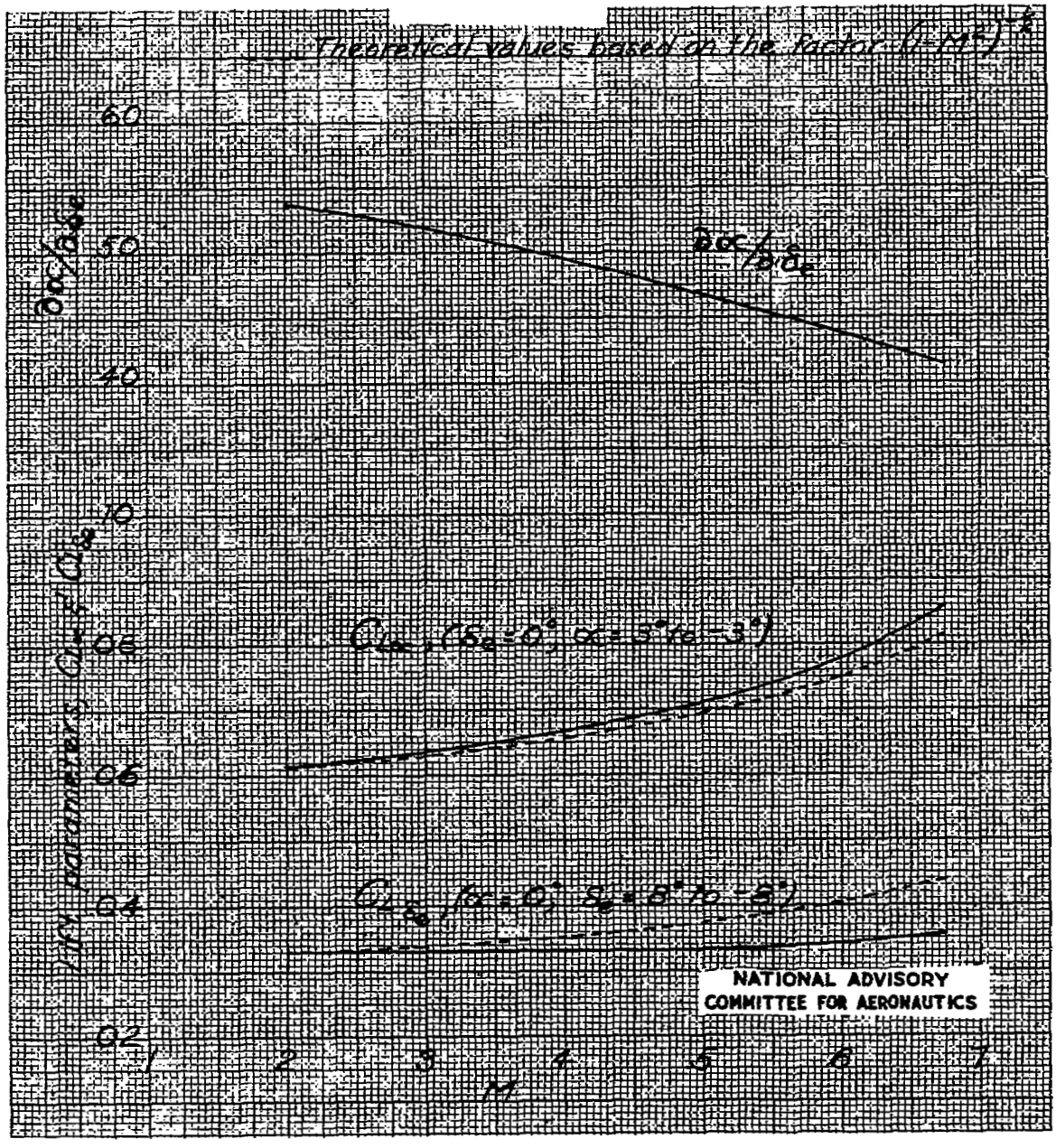

Figure 7.- Variation of the lift parameters and elevator effectiveness with Mach number.

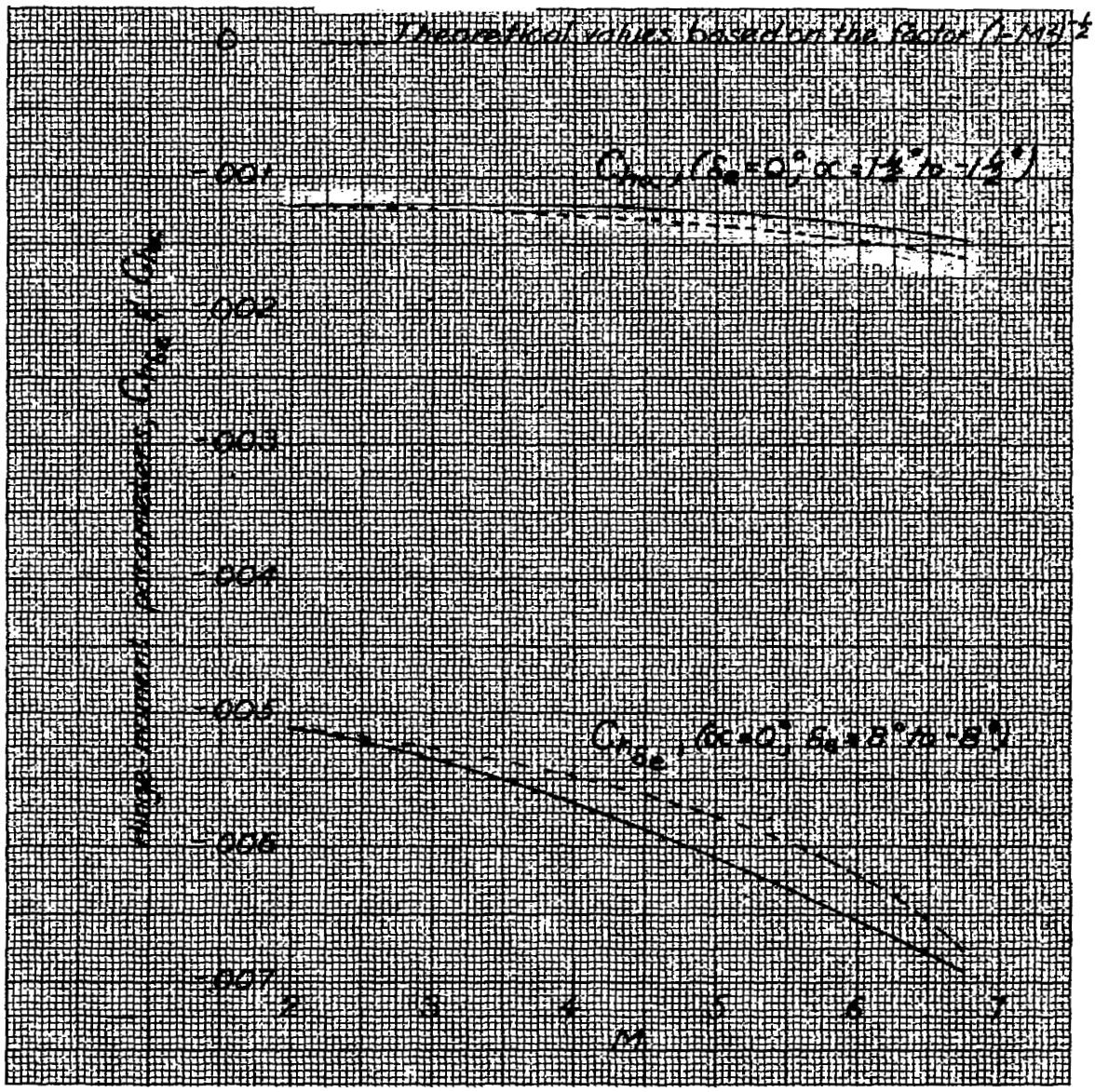

NATIONAL ADVISORY
COMMITTEE FOR AERONAUTICS

Figure 8.- Variation of the hinge-moment parameters with Mach number.

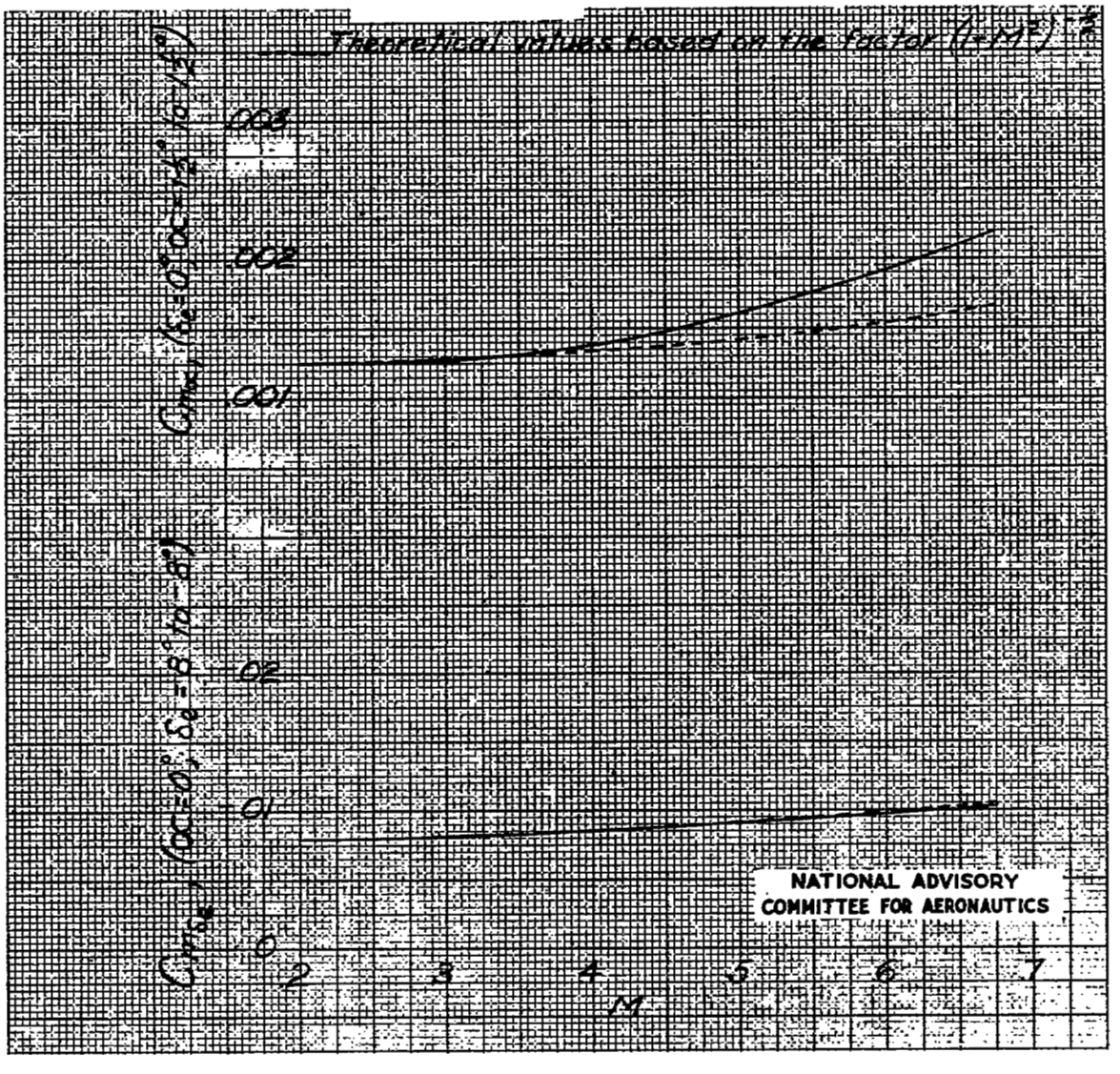

Figure 9.- Variation of the pitching-moment parameters with Mach number.

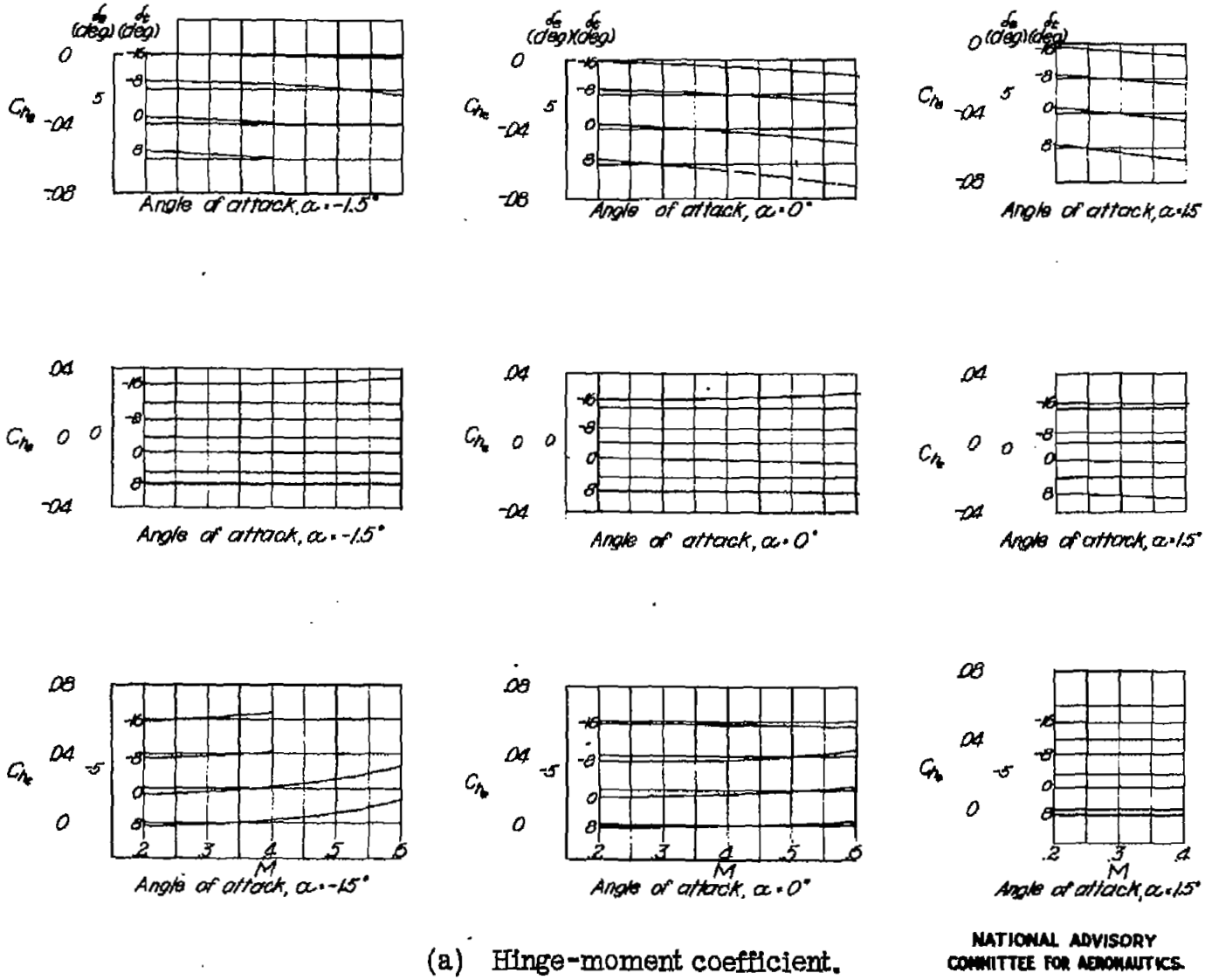

(a) Hinge-moment coefficient.

NATIONAL ADVISORY COMMITTEE FOR AERONAUTICS.

Figure 10.- Variation of the aerodynamic characteristics with Mach number for various trim-tab angles.

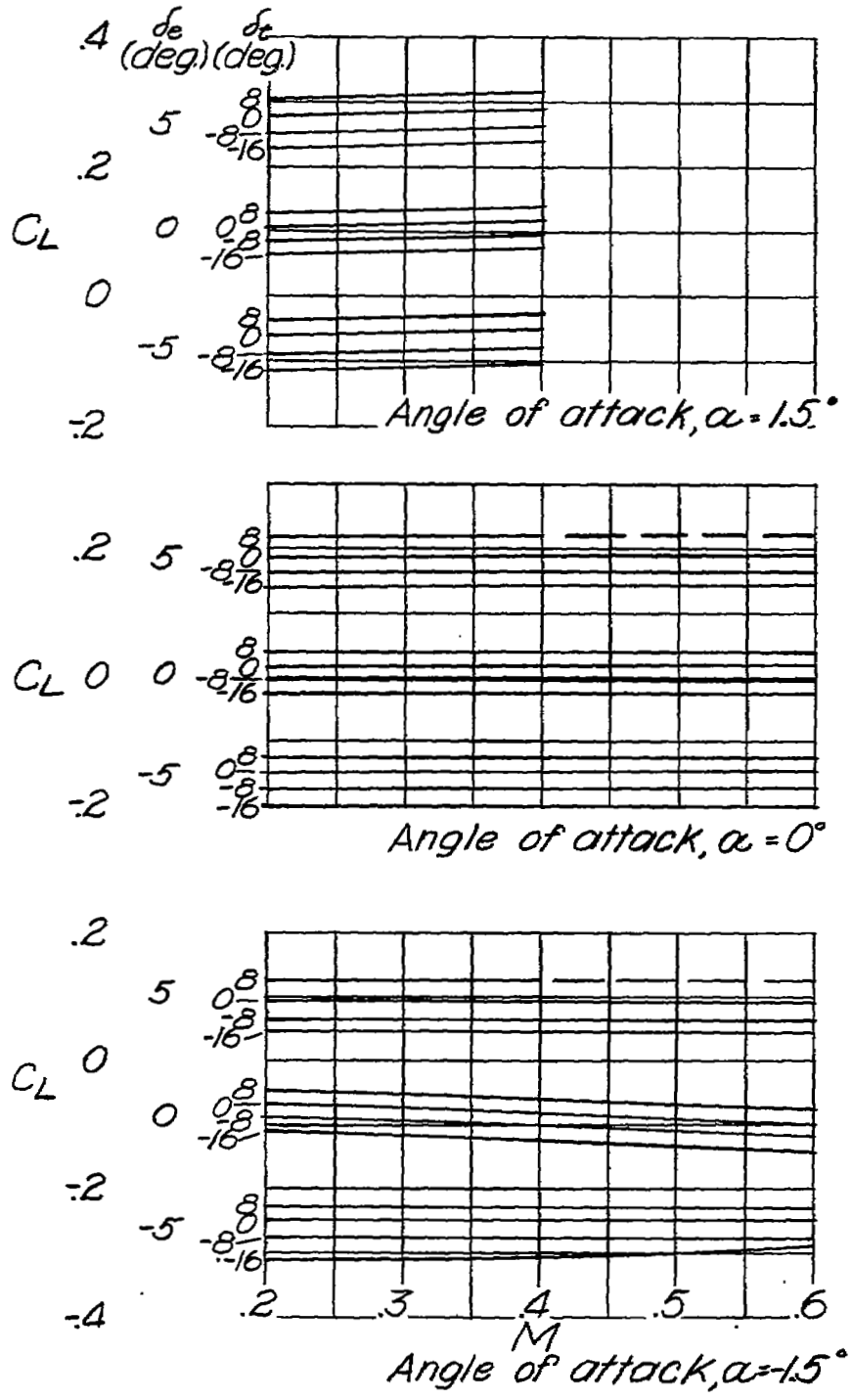

NATIONAL ADVISORY COMMITTEE FOR AERONAUTICS.

(b) Lift coefficient.

Figure 10.- Continued.

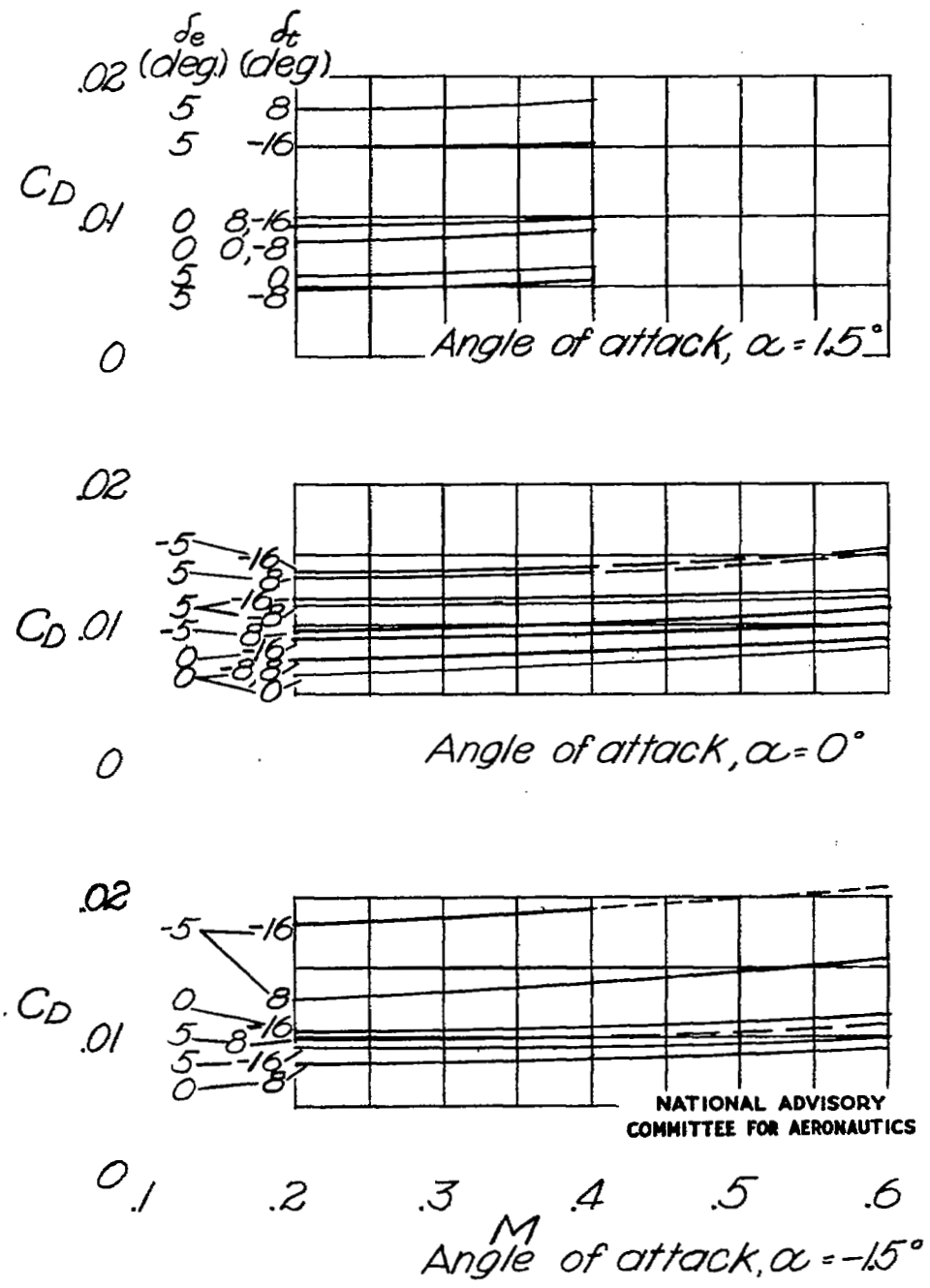

(c) Drag coefficient.

Figure 10.- Continued.

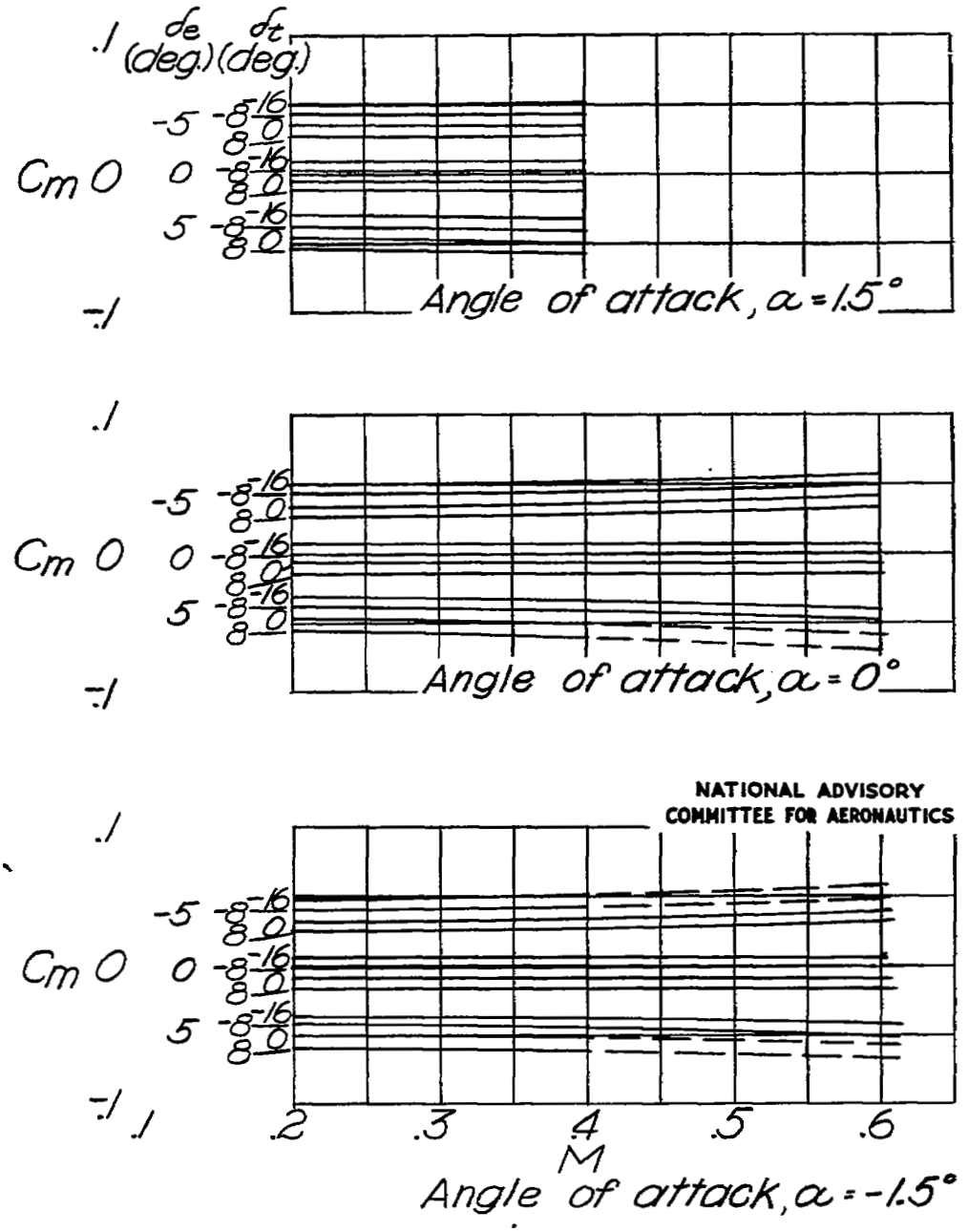

(d) Pitching-moment coefficient.

Figure 10.- Concluded.

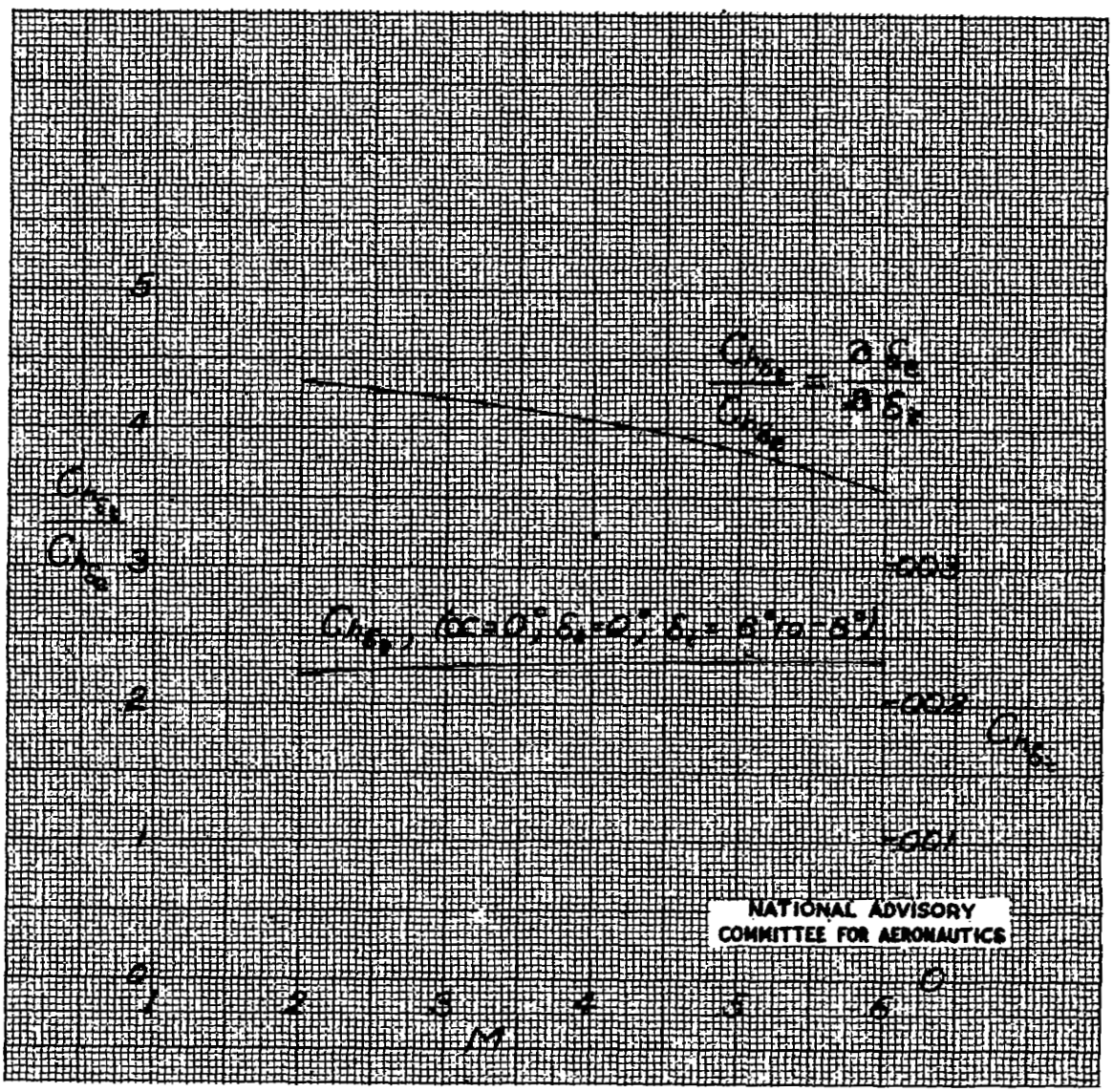

Figure 11.- Variation of the elevator trim-tab effectiveness parameters with Mach number.

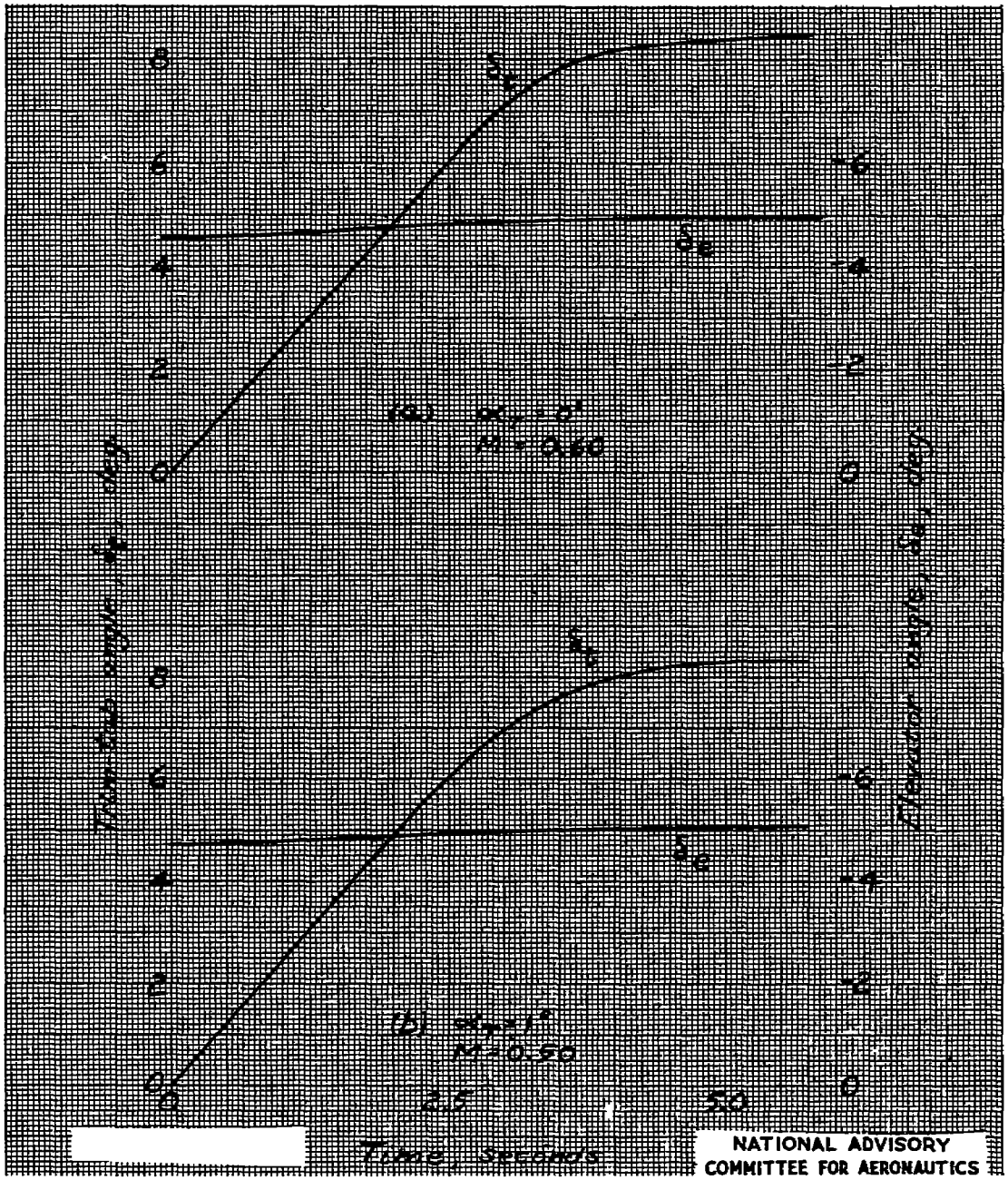

Figure 12.- Change in trim-tab angle with time.

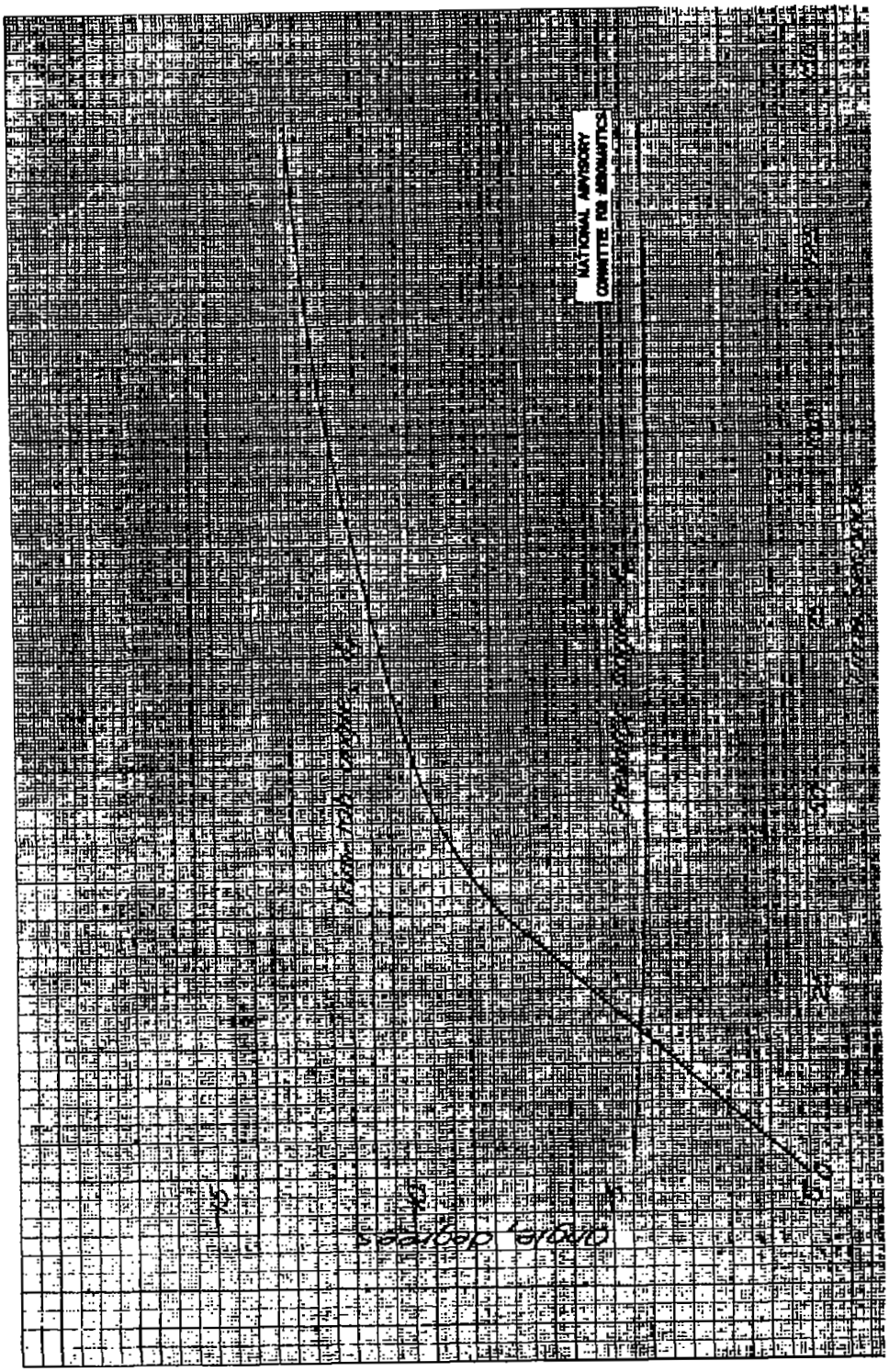

Figure 13.- Change in trim-tab angle with time, $\alpha_T = 0^\circ$, M = 0.6.

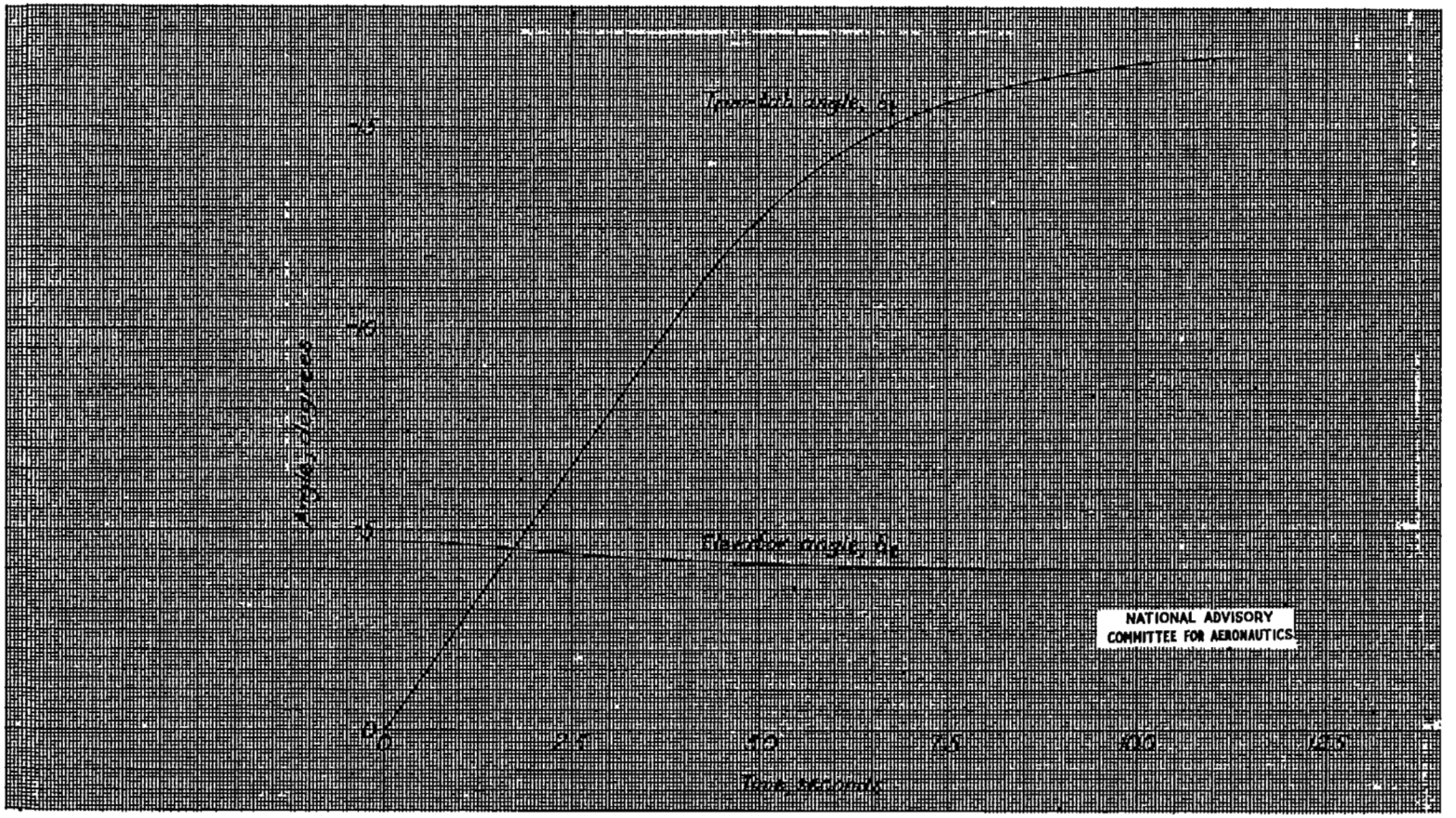

Figure 14.- Change in trim-tab angle with time. $\alpha_T = 1^\circ$, M = 0.50.

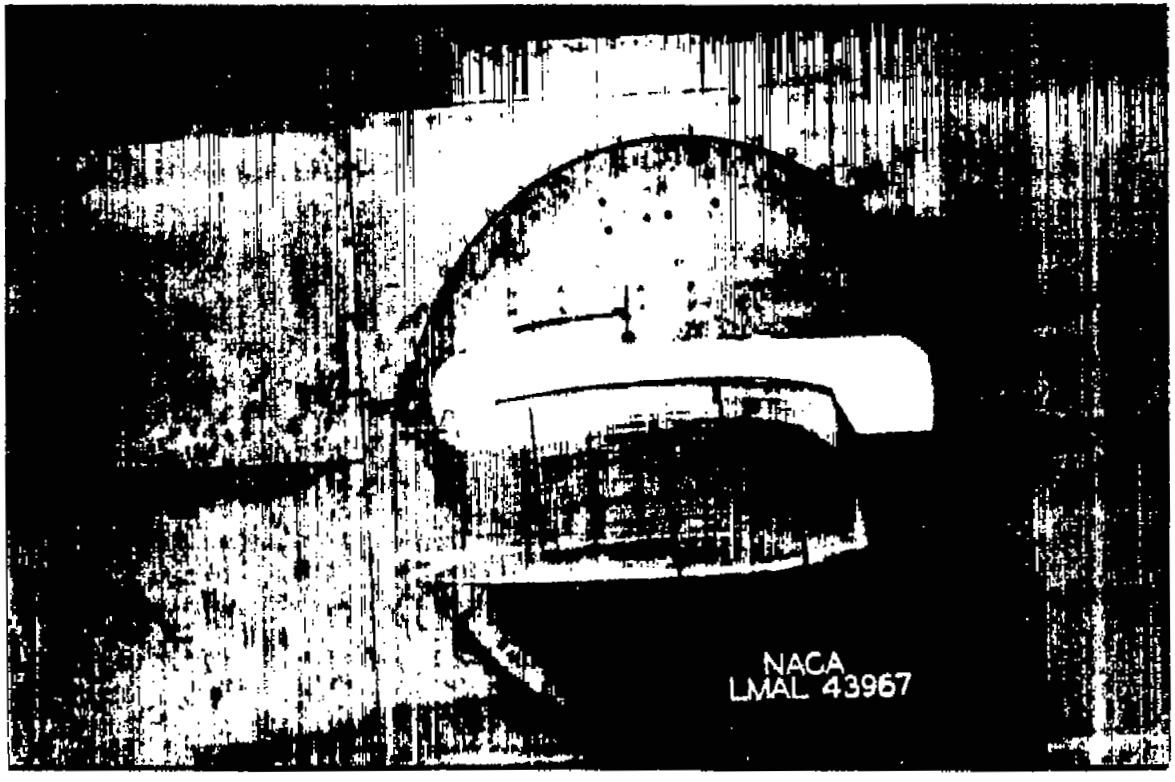

Figure 15.- View of lower surface of the horizontal tail; zero aerodynamic load. Stabilizer $P_i = 0$.

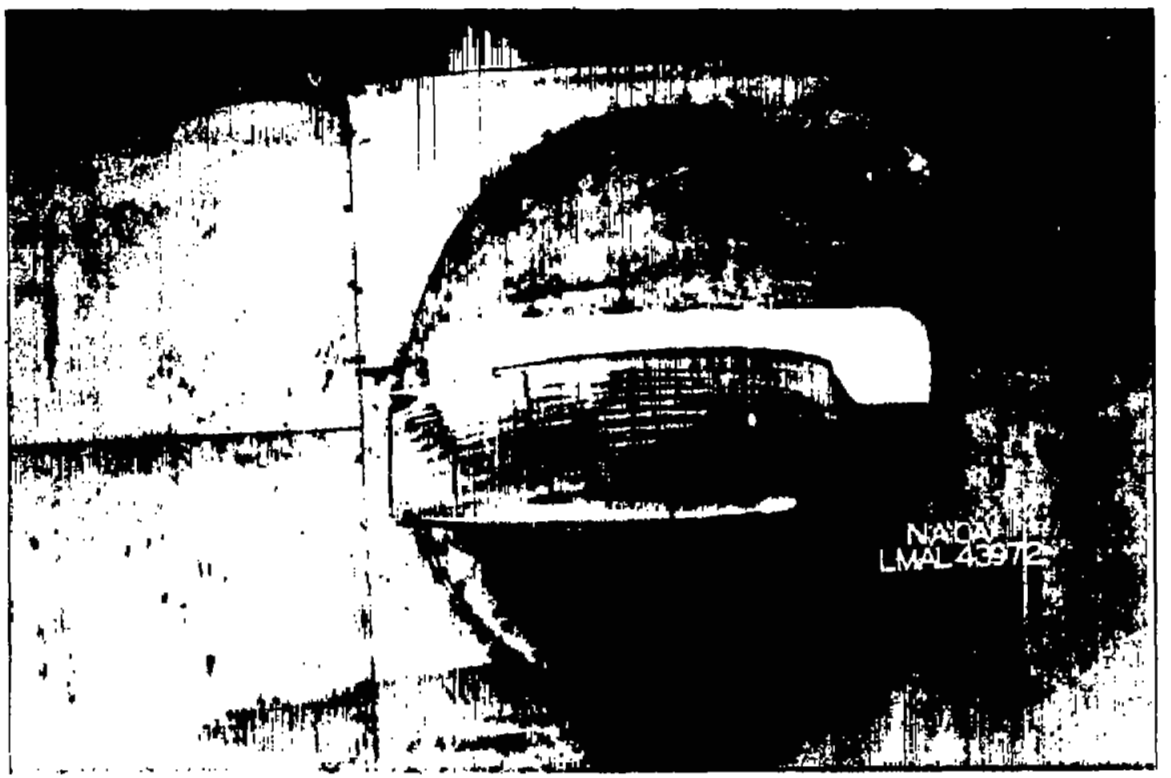

Figure 16.- Skin deflections on the lower surface of the horizontal tail. $\alpha_T = 0^\circ$, $\delta_e = -5^\circ$, $\delta_t = 0^\circ$, M = 0.600, Stabilizer $P_i = 0.012$.

(a) $\alpha_T = 0^\circ$.

Figure 17.- Skin deflections on the lower surface of the horizontal tail. $\delta_e = 0^\circ$, $\delta_t = 0^\circ$, M = 0.400, Stabilizer $P_i = 0.011$.

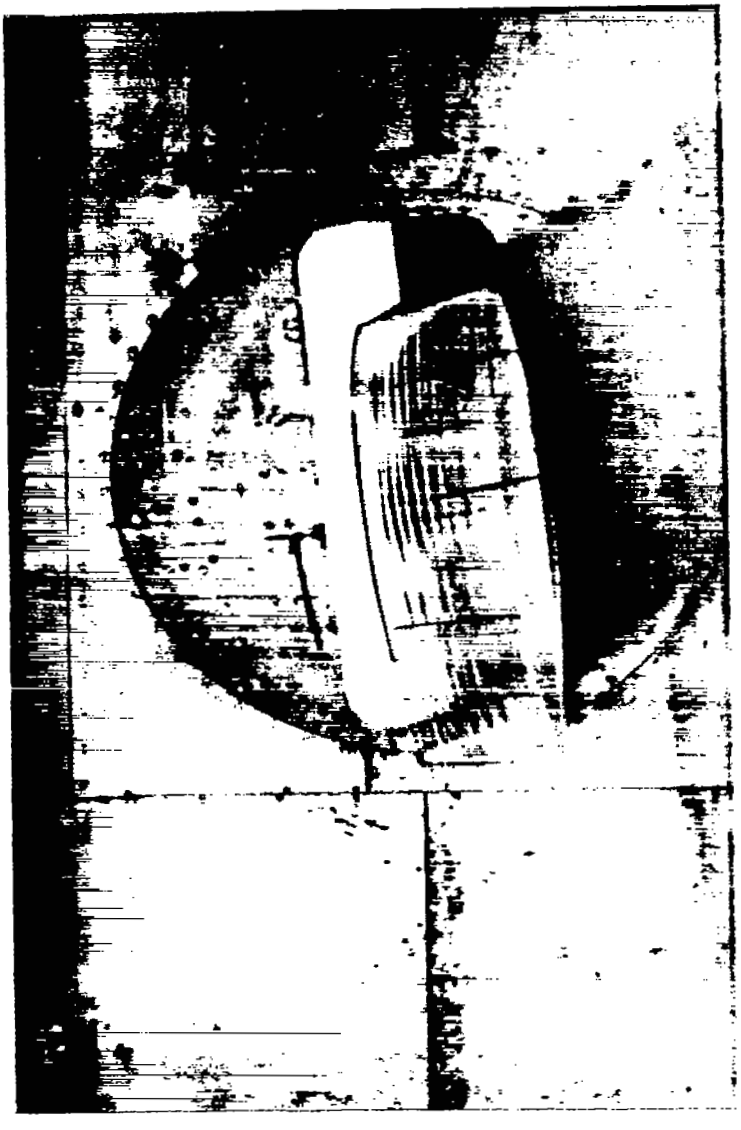

(b) $\alpha_T = -6^\circ$.

Figure 17.- Concluded.